Clim. Past Discuss., 10, 3537–3584, 2014
www.clim-past-discuss.net/10/3537/2014/
doi:10.5194/cpd-10-3537-2014

Climate of the Past
Discussions
Open Access

The WAIS-Divide deep ice core WD2014 chronology – Part 2: Methane synchronization (68–31 ka BP) and the gas age-ice age difference

C. Buizert[1], K. M. Cuffey[2], J. P. Severinghaus[3], D. Baggenstos[3], T. J. Fudge[4], E. J. Steig[4], B. R. Markle[4], M. Winstrup[4], R. H. Rhodes[1], E. J. Brook[1], T. A. Sowers[5], G. D. Clow[6], H. Cheng[7,8], R. L. Edwards[8], M. Sigl[9], J. R. McConnell[9], and K. C. Taylor[9]

[1]College of Earth, Ocean, and Atmospheric Sciences, Oregon State University, Corvallis, OR 97331, USA
[2]Department of Geography, University of California, Berkeley, CA 94720, USA
[3]Scripps Institution of Oceanography, University of California, San Diego, La Jolla, CA 92093, USA
[4]Quaternary Research Center and Department of Earth and Space Sciences, University of Washington, Seattle, WA 98195, USA
[5]Department of Geosciences and Earth and Environmental Systems Institute, Pennsylvania State University, University Park, PA 16802, USA
[6]US Geological Survey, Boulder, CO 80309, USA

[7]Institute of Global Environmental Change, Xi'an Jiaotong University, Xi'an 710049, China
[8]Department of Geology and Geophysics, University of Minnesota, Minneapolis, MN 55455, USA
[9]Desert Research Institute, Nevada System of Higher Education, Reno, NV 89512, USA

Received: 1 August 2014 – Accepted: 11 August 2014 – Published: 28 August 2014

Correspondence to: C. Buizert (buizertc@science.oregonstate.edu)

Published by Copernicus Publications on behalf of the European Geosciences Union.

Abstract

The West Antarctic Ice Sheet (WAIS)-Divide ice core (WAIS-D) is a newly drilled, high-accumulation deep ice core that provides Antarctic climate records of the past ∼ 68 ka at unprecedented temporal resolution. The upper 2850 m (back to 31.2 ka BP) have been dated using annual-layer counting. Here we present a chronology for the deep part of the core (67.8–31.2 ka BP), which is based on stratigraphic matching to annual-layer-counted Greenland ice cores using globally well-mixed atmospheric methane. We calculate the WAIS-D gas age-ice age difference (Δage) using a combination of firn densification modeling, ice flow modeling, and a dataset of δ^{15}N-N$_2$, a proxy for past firn column thickness. The largest Δage at WAIS-D occurs during the last glacial maximum, and is 525 ± 100 years. Internally consistent solutions can only be found when assuming little-to-no influence of impurity content on densification rates, contrary to a recently proposed hypothesis. We synchronize the WAIS-D chronology to a linearly scaled version of the layer-counted Greenland Ice Core Chronology (GICC05), which brings the age of Dansgaard-Oeschger (DO) events into agreement with the U/Th absolutely dated Hulu speleothem record. The small Δage at WAIS-D provides valuable opportunities to investigate the timing of atmospheric greenhouse gas variations relative to Antarctic climate, as well as the interhemispheric phasing of the bipolar "seesaw".

1 Introduction

Deep ice cores from the polar regions provide high-resolution climate records of past atmospheric composition, aerosol loading and polar temperatures (e.g. NGRIP community members, 2004; EPICA Community Members, 2006; Wolff et al., 2006; Ahn and Brook, 2008). Furthermore, the coring itself gives access to the ice sheet interior and bed, allowing investigation of glaciologically important processes such as ice deformation (Gundestrup et al., 1993), folding (NEEM community members, 2013), crystal

CPD
10, 3537–3584, 2014

fabric evolution (Gow et al., 1997) and geothermal heat flow (Dahl-Jensen et al., 1998). Having a reliable ice core chronology (i.e., an age-depth relationship) is paramount for the interpretation of the climatic records and comparison to marine and terrestrial paleoclimatic archives.

The West Antarctic Ice Sheet (WAIS) Divide ice core (WAIS-D, 79.48° S, 112.11° W, 1766 m a.s.l., –30 °C present day mean annual temperature) was drilled and recovered to 3404 m depth (WAIS-Divide Project Members, 2013). Drilling was stopped 50 m above the estimated bedrock depth to prevent contamination of the basal hydrology. Due to high accumulation rates of 22 cm ice a^{-1} at present and ~ 10 cm ice a^{-1} during the last glacial maximum (LGM), the WAIS-D core has the potential to deliver climate records of unprecedented temporal resolution (Steig et al., 2013; Sigl et al., 2013) as well as gas records that are only minimally affected by diffusive smoothing in the firn column (Mischler et al., 2009; Mitchell et al., 2011, 2013). The combination of high accumulation rates and basal melting at the WAIS-D site results in ice near the bed that is relatively young (~ 68 ka) compared to cores drilled in central East Antarctica.

In WAIS-D, annual layers can be identified reliably for the upper 2850 m of the core, reaching back to 31.2 ka BP (thousands of years before present, with present defined as 1950 C.E.). Below 2850 m depth an alternative dating strategy is needed. Several methods have been employed previously at other deep ice core sites. First, orbital tuning via $\delta O_2/N_2$ has been applied successfully to several Antarctic cores (Bender, 2002; Kawamura et al., 2007). However, the short WAIS-D age span of only ~ 3 precessional cycles, in combination with the low signal-to-noise ratio of $\delta O_2/N_2$ data, makes this technique unsuitable for WAIS-D. The uncertainty in the orbital tuning is about one fourth of a precessional cycle (~ 5 ka), making it a relatively low-resolution dating tool. Second, in Greenland, ice flow modeling has been used to extend layer-counted chronologies (e.g., Johnsen et al., 2001; Wolff et al., 2010). This method requires assumptions about past accumulation rates, ice flow and ice sheet elevation. Particularly for the oldest WAIS-D ice, the resulting uncertainty would be substantial. Third, several radiometric techniques have been proposed to date ancient ice. Radiocarbon (^{14}C)

CPD
10, 3537–3584, 2014

dating of atmospheric CO_2 trapped in the ice is unsuitable as it suffers from in-situ cosmogenic production in the firn (Lal et al., 1990), and the oldest WAIS-D ice dates beyond the reach of ^{14}C dating. Other absolute (radiometric) dating techniques, such as recoil ^{234}U dating (Aciego et al., 2011), ^{81}Kr dating (Buizert et al., 2014) or atmospheric ^{40}Ar build-up (Bender et al., 2008) currently suffer from uncertainties that are too large (≥ 20 ka) to make them applicable at WAIS-D.

Instead, at WAIS-D we use stratigraphic matching to well-dated Greenland ice cores using globally well-mixed atmospheric methane (CH_4) mixing ratios (Blunier et al., 1998, 2007; Blunier and Brook, 2001; Capron et al., 2010; Petrenko et al., 2006). This method is particularly suited to WAIS-D because of the small gas age-ice age difference (Δage, Sect. 3) and the high-resolution, high-precision CH_4 record available (Sect. 2.1). The method has three main sources of uncertainty: (i) the age uncertainty in the records one synchronizes to, (ii) Δage of the ice core being dated, and (iii) the interpolation scheme used in between the CH_4 tie-points. We present several improvements over previous work that reduce and quantify these uncertainties: (i) we combine the layer-counted Greenland Ice Core Chronology (GICC05) and a recently updated version of the U/Th-dated Hulu speleothem record to obtain a more accurate estimate of the (absolute) ages of abrupt Dansgaard-Oeschger (DO) events (Sect. 4.4); (ii) we combine firn densification modeling, ice flow modeling, a new WAIS-D $\delta^{15}N$-N_2 dataset that spans the entire core, and a Monte Carlo sensitivity study to obtain a reliable Δage estimate (Sect. 3); and (iii) we compare four different interpolation schemes to obtain an objective estimate of the interpolation uncertainty (Sect. 4.5).

This work is the second part in a series of two papers describing the WD2014 chronology for the WAIS-D core in detail. The first part describes the development of the annual layer count from both multi-parameter chemistry and electrical conductivity measurements (Sigl et al., 2014b). The WD2014 chronology is currently the recommended gas and ice timescale for the WAIS-D deep core, and as such supersedes the previously published WDC06A-7 chronology (WAIS-Divide Project Members, 2013).

CPD
10, 3537–3584, 2014

2 Methods

2.1 Data description

Measurements of water stable isotopes. Water isotopic composition (δ^{18}O and δD = δ^{2}H) was measured at IsoLab, University of Washington. Procedures for the deep section of the core are identical to those used for the upper part of the core reported in WAIS-Divide Project Members (2013); Steig et al. (2013). Measurements were made at 0.25 to 0.5 m depth resolution using laser spectroscopy (Picarro L2120-*i* water isotope analyzer), and normalized to VSMOW-SLAP (Vienna Standard Mean Ocean Water – Standard Light Antarctic Precipitation).

Measurements of CH_4. Two CH_4 datasets were used for WAIS-D. The first is from discrete ice samples, and was measured jointly at Penn State University (0–68 ka, 0.5–2 m resolution) and at Oregon State University (11.4–24.8 ka, 1–2 m resolution). Air was extracted from ~ 50 gram ice samples using a melt-refreeze technique, and analyzed on a standard gas chromatograph equipped with a flame-ionization detector. Corrections for solubility, blank size and gravitational enrichment are applied (Mitchell et al., 2011; WAIS-Divide Project Members, 2013). The second dataset is a continuous CH_4 record measured by coupling a laser spectrometer to a continuous flow analysis setup (Stowasser et al., 2012; Rhodes et al., 2013), and was measured jointly by Oregon State University and the Desert Research Institute (Rhodes et al., 2014). The continuous dataset is used to identify the abrupt DO transitions, as it provides better temporal resolution and analytical precision. Both records are reported on the NOAA04 scale (Dlugokencky et al., 2005).

Measurements of δ^{15}N. Atmospheric N_2 isotopic composition (δ^{15}N) was measured at Scripps Institution of Oceanography, University of California. Air was extracted from ~ 12 gram ice samples using a melt-refreeze technique, and collected in stainless steel tubes at liquid-He temperature. δ^{15}N was analyzed using conventional dual-inlet Isotope Ratio Mass Spectrometry (IRMS) on a Thermo Finnigan Delta V mass spectrometer. Results are normalized to La Jolla (California, USA) air, and routine analytical

CPD
10, 3537–3584, 2014

corrections are applied (Sowers et al., 1989; Petrenko et al., 2006; Severinghaus et al., 2009).

Measurements of [Ca]. Ca concentrations in the ice were measured at the Ultra Trace Chemistry Laboratory at the Desert Research Institute via continuous flow analysis. Longitudinal samples of ice (approximately 100 cm × 3.3 cm × 3.3 cm) were melted continuously on a melter head that divides the melt water into three parallel streams. Elemental measurements were made on melt water from the innermost part of the core with ultra-pure nitric acid added to the melt stream immediately after the melter head; potentially contaminated water from the outer part of the ice is discarded. Elemental analysis of the innermost melt water stream is performed in parallel on two inductively coupled plasma mass spectrometers (ICPMS), each measuring a different set of elements; some elements were analyzed on both. The dual ICPMS setup allows for measurement of a broad range of 30 elements and data quality control (McConnell et al., 2002, 2007). Continuous Ca and CH_4 measurements are done on the same ice, and are exactly co-registered in depth.

2.2 Firn densification model description

Air exchange with the overlying atmosphere keeps the interstitial air in the porous firn layer younger than the surrounding ice matrix, resulting in an age difference between polar ice and the gas bubbles it contains, commonly referred to as Δage (Schwander and Stauffer, 1984). Here we use a coupled firn densification – heat diffusion model to calculate Δage back in time (Barnola et al., 1991; Goujon et al., 2003; Schwander et al., 1997; Rasmussen et al., 2013), constrained by measurements of $\delta^{15}N$ of N_2, a proxy for past firn column thickness (Sowers et al., 1992). The model is based on a dynamical description of the Herron-Langway model formulated in terms of overburden load (Herron and Langway, 1980), which is solved in a Lagrangian reference frame. This model has already been applied successfully to the Greenland NEEM and GISP2 cores (Rasmussen et al., 2013; Seierstad et al., 2014), where it gives a good agreement to the Goujon densification model (Rasmussen et al., 2013; Goujon et al., 2003).

The model allows for the inclusion of softening of firn in response to impurity loading (Horhold et al., 2012), following the mathematical description of Freitag et al. (2013a). The equations governing the model densification rates are given in Appendix A.

The model uses a 2 year time step and 0.5 m depth resolution down to 1000 m, the lower model boundary. A thick model domain is needed because of the long thermal memory of the ice sheet. At WAIS-D, downward advection of cold surface ice is strong due to the relatively high accumulation rates, and the geothermal gradient does not penetrate the firn column (Cuffey and Paterson, 2010). We further use a lock-in density that equals the mean close-off density (Martinerie et al., 1994) minus 17.5 $kg\,m^{-3}$ (as in Blunier and Schwander, 2000), and an empirical parameterization of lock-in gas age based on firn air measurements from 10 sites (Buizert et al., 2012, 2013). We use the steady state version of the Herron-Langway model (Herron and Langway, 1980) in performing sensitivity studies (Sect. 3.2).

3 The gas age-ice age difference (Δage)

3.1 The WD2014 Δage reconstruction

The firn densification forward model uses past surface temperature $T(t)$ and accumulation $A(t)$ as model forcings, and provides $\Delta age(t)$ and $\delta^{15}N(t)$ as model output.

Our temperature reconstruction (Fig. 1a) is based on water δD, a proxy for local vapor condensation temperature, calibrated using a measured borehole temperature profile (following Cuffey et al., 1995; Cuffey and Clow, 1997) and, for the last 31.2 ka, adjusted iteratively to satisfy constraints on firn thickness provided by $\delta^{15}N$ and by the observed layer thickness $\lambda(z)$. This borehole temperature calibration approach is possible at WAIS-D because the large ice thickness and relatively high accumulation rates help to preserve a memory of past temperatures in the ice sheet. A coupled 1-D ice flow-heat diffusion model converts surface $T(t)$ into a depth profile for comparison to measured borehole temperatures (WAIS-Divide Project Members, 2013). Details of

CPD
10, 3537–3584, 2014

the temperature optimization process and 1-D flow modeling will be provided elsewhere (Cuffey et al., 2014).

For the past 31.2 ka WAIS-D has an annual layer counted chronology; for this period the annual layer thickness $\lambda(z)$ provides a constraint on past accumulation rates via $\lambda(z) = A(z) \times f(z)$, where $f(z)$ is the (modeled) ice-flow thinning function (Cuffey and Paterson, 2010). The thinning function corresponds to the ratio of the annual layer thickness at depth in the ice sheet to the original thickness of that layer at the time of deposition (in m ice equivalent). WAIS-D accumulation reconstructed from $\lambda(z)$ is plotted in black in Fig. 1b, where $f(z)$ is calculated with the ice flow model used in the borehole temperature calibration.

Prior to 31.2 ka we have no such constraint on $A(t)$, and an alternative approach is needed. We use the densification model as an inverse model, where we ask the model to find the $A(t)$ history that minimizes the root mean square deviation between measured and modeled $\delta^{15}N$, given the $T(t)$ forcing. The $\delta^{15}N$ data and model fit are shown in Fig. 1c, the $A(t)$ history that optimizes the $\delta^{15}N$ fit is shown in Fig. 1b (red), and the modeled Δage is shown in Fig. 1c (orange). The optimal $A(t)$ history is estimated in two steps. First we make an initial estimate $A_{init}(t)$ for the past accumulation history. Second, we adjust the $A(t)$ forcing by applying a smooth perturbation $\xi(t)$ such that $A(t) = [1 + \xi(t)] \times A_{init}(t)$; an automated algorithm is used to find the curve $\xi(t)$ that optimizes the model fit to the $\delta^{15}N$ data. For the last 31.2 ka we obtain a good agreement between A obtained from $\lambda(z)$ and the modeled $f(z)$ (Fig. 1b, black) and A obtained from the inverse method (red). The solution we present here is therefore fully internally consistent, i.e., the A and T histories used in the firn densification modeling are the same as those used in the ice-flow modeling, and they provide a good fit to both the $\delta^{15}N$ data and borehole temperature data. WAIS-D does not suffer from the $\delta^{15}N$ model-data mismatch that is commonly observed for East Antarctic cores during the glacial period (Landais et al., 2006).

We base our A_{init} values on $\lambda(z)$ for the past 31.2 ka; prior to that we use the common assumption that A follows $\delta^{18}O$ (i.e., Clausius-Clapeyron scaling); the fit to the $\delta^{15}N$

CPD
10, 3537–3584, 2014

data is optimized for $A = 24.2 \times \exp[0.1263 \times \delta^{18}\mathrm{O}]$. To test the validity of the Clausius-Clapeyron assumption, we additionally run the scenario $A_{\mathrm{init}}(t) = 0.22\,\mathrm{m\,a^{-1}}$ (i.e., constant accumulation at present day level). The $A(t)$ and Δage reconstructed under both A_{init} scenarios are similar at multi-millennial timescales (Fig. 2). In the layer counted interval (< 31.2 ka BP), A obtained from $\lambda(z)$ and δ^{18}O are significantly coherent at all timescales longer than 3000 years, but not at higher frequencies. This is equivalent to the variability resolved in the $A_{\mathrm{init}}(t) = 0.22\,\mathrm{m\,a^{-1}}$ scenario above. We conclude that the WAIS-D δ^{15}N data support the idea that A follows δ^{18}O on multi-millennial timescales. However, there may not be a strong relationship at timescales less than a few thousand years, as is clear from the abrupt A increase around 12 ka seen in $\lambda(z)$ that is not reflected in δ^{18}O (Fig. 1a and b). For consistency between the upper and deeper part of the core we use the Δage values obtained with the inverse densification model for the entire core.

Recently another δ^{15}N-based approach has been suggested that uses Δdepth, rather than Δage, in reconstructing gas chronologies (Parrenin et al., 2012). This method removes the dependence on $T(t)$, and replaces this by a dependence on the thinning function $\lambda(z)$. Note that this method is very successful in the upper part of an ice core where $\lambda(z)$ is well constrained, but not very reliable near the base where $\lambda(z)$ is highly uncertain. Therefore, the firn densification modeling approach should be considered to be more reliable at WAIS-D during Marine Isotope Stage (MIS) 2 through 4. Results from the Δdepth method are plotted in black in Fig. 1c, and generally show good agreement with the firn modeling approach. A notable exception is the 60–65 ka interval, where the Δdepth method overestimates the Δage due to the fact that we have to compress $\lambda(z)$ strongly in order to fit age constraints derived from DO 18 (Sect. 4.5).

Last, we want to point out that the δ^{15}N data support an early warming at WAIS-D as reported recently by WAIS-Divide Project Members (2013). WAIS-D δ^{15}N starts to decrease around 20.5 ka BP, suggesting a thinning of the firn column. The $\lambda(z)$ (as derived from the layer count) shows that accumulation did not change until 18 ka BP, at which point it started to increase (which would act to increase the firn thickness).

The most plausible explanation for the $\delta^{15}N$ decrease around 20.5 ka BP is therefore an early onset of West-Antarctic deglacial warming, in agreement with increasing $\delta^{18}O$ around that time. The warming enhances the densification rate of polar firn, thereby decreasing its thickness (e.g., Herron and Langway, 1980).

3.2 Δage sensitivity study

Besides A and T there are several model parameters that have the potential to influence the model outcome; these are the convective zone (CZ) thickness (Sowers et al., 1992; Kawamura et al., 2006), surface density (ρ_0), and sensitivity to ice impurity content. In this section we evaluate the sensitivity of the model output to all of these parameters. We performed 1000 model runs in which the model parameters were randomly perturbed. The spread in Δage model results is used to calculate the WD2014 age uncertainty.

Convective Zone thickness. In the WD2014 model run (Sect. 3.1) we use a constant 3.5 m CZ, corresponding to the present day situation (Battle et al., 2011). In the sensitivity study we vary the CZ by one of two methods: (1) We let the CZ be constant in time; its thickness is set by drawing from a Gaussian distribution with 3.5 m mean, and 3.5 m 2σ width (i.e., 95 % probability of drawing a value in the 0–7 m range). (2) We let the CZ be a function of accumulation rate (Dreyfus et al., 2010), $CZ = 3.5 + k \times (A - 0.22)$; we draw k from a Gaussian distribution with mean of -10 and a 2σ width of 40 (at an LGM A of 10 cm a^{-1} this gives a CZ of 0–10 m thickness). In both methods, whenever CZ values are selected that are smaller than 0 m, the CZ thickness is set to 0 m instead. For each of the 1000 model runs in the sensitivity study we randomly selected either of the two methods.

Surface density. In the WD2014 model run we use past surface densities (ρ_0) as given by the parameterization of Kaspers et al. (2004). In the sensitivity study we add a constant offset to the Kaspers values, the magnitude of which is drawn from a Gaus-

CPD
10, 3537–3584, 2014

sian distribution of zero mean and a 2σ width of $60\,\mathrm{kg\,m^{-3}}$. This range corresponds to the full range of observed ρ_0 variability in Kaspers et al. (2004).

Past temperatures. Model temperature forcing is constrained by δD and measured borehole temperatures. There is, however, a range of solutions allowed by the borehole temperature and ice-flow model; here we use the upper and lower extremes of this range, determined by Monte Carlo analysis using uncertainties of input variables. The scenarios were chosen to provide the maximum T range for the glacial period rather than for the Holocene, because we are interested in the uncertainty in the methane synchronization (68–31.2 ka BP). In the sensitivity study we use $T(t) = T_{\mathrm{optimal}}(t) + \kappa \times \Delta T(t)$, where T_{optimal} is the forcing used in the WD2014 model run (Fig. 1a), $\Delta T(t)$ is half the difference between the maximum-T and minimum-T scenarios, and κ is drawn from a Gaussian distribution of zero mean and unit 2σ width (giving 95 % probability that $T(t)$ is within the extreme range identified from the borehole, Fig. 3a).

δ^{15}N uncertainty. Duplicates were not run for most δ^{15}N data in this study, but the pooled standard deviations of Holocene WAIS Divide δ^{15}N data sets with duplicate analyses are 0.003 ‰ (Orsi, 2013). We conservatively adopt an analytical uncertainty of 0.005 ‰ for this data set to allow for other sources of error, including possible hydrocarbon interference from an event that brought pump oil into the mass spectrometer. In addition, the interpretation of δ^{15}N in terms of firn thickness is subject to further uncertainty due to irregular firn layering and the stochastic nature of bubble trapping, as was observed for other atmospheric gases in Etheridge et al. (1992); Rhodes et al. (2013). For each run of the sensitivity study, we therefore perturb each of the individual δ^{15}N data points by adding an offset that is drawn from a Gaussian distribution of zero mean and a 2σ width of 0.015 ‰.

Impurity-enhanced densification. Following recent work we include the possibility that increased glacial impurity loading could have enhanced densification rates (Horhold et al., 2012; Freitag et al., 2013a). We use the mathematical formulation of Freitag et al. (2013a), in which the activation energy of the sintering process is a function of the Ca concentration in the firn. The value of β, the sensitivity to Ca, is drawn

CPD
10, 3537–3584, 2014

from a Gaussian distribution with 0.0015 mean and a 2σ width of 0.0015. The topic of impurity-enhanced densification is discussed in detail in Sect. 3.3.

The A and Δage scenarios found in the sensitivity study are shown in Fig. 3b and c, respectively. The shaded areas in Fig. 3b and c give the total range of solutions, as well as the $\pm 2\sigma$ and $\pm 1\sigma$ confidence intervals. Note that the total range of solutions will depend on the number of model runs (here 1000), but the position of the $\pm 2\sigma$ and $\pm 1\sigma$ envelopes does not. To investigate the distribution of values, we include histograms of Δage at 20 ka intervals (Fig. 3d–f). Based on the sensitivity study, we estimate the WAIS-D Δage to be 525 ± 100 years (2σ uncertainty) at the last glacial maximum (LGM, $\sim$ 20 ka BP). The Δage value of (345 ± 55 years) at 40 ka BP gives a representative Δage for MIS 3.

3.3 Impurity softening of firn?

Recent work suggests a link between densification rates and impurity content (for which $[Ca^{2+}]$ is used as a proxy) in polar firn (Horhold et al., 2012; Freitag et al., 2013a). Here we measured total [Ca] by ICP-MS, but at WAIS-D nearly all Ca is in the form of Ca^{2+}. The influence of the impurity sensitivity β (see Eq. (A6) in the Appendix) on Δage at WAIS-D is shown in Fig. 4. The sensitivity recommended by Freitag et al. (2013a) from investigating present day firn packs is $\beta = 1 \times 10^{-2}$. We reconstructed A and Δage with the firn densification inverse model using five values of β ranging from $\beta = 0$ (red) to $\beta = 1 \times 10^{-2}$ (blue) in steps of 2.5×10^{-3}. Average [Ca] is around 0.8 ng g^{-1} in the early Holocene and around 9 ng g^{-1} in the LGM, about an order of magnitude change. Following Freitag et al. (2013a) we use the total [Ca], rather than non-sea salt Ca. If densification rates are sensitive to impurity loading (large β, blue curves), this results in increased firn compaction during the LGM. The densification model, which is trying to match the $\delta^{15}N$ data, will compensate by increasing the A forcing, which in turn results in a decreasing Δage. Hence the model simulations with large β (blue) give a higher A and smaller Δage.

CPD
10, 3537–3584, 2014

For the past 31.2 ka we have an independent A estimate from $\lambda(z)$, that we can compare to the solutions from the firn model (Fig. 4, black curve). We also plotted Δage reconstructed via the Δdepth method of Parrenin et al. (2012). Remarkably, we find consistent solutions only when using a Ca sensitivity $\beta \leq 2.5 \times 10^{-3}$, i.e., less than one quarter of the sensitivity suggested by Freitag et al. (2013a). The best fit to the independent LGM (25–20 ka BP) A and Δage estimates is obtained for $\beta = 0$. We conclude that WAIS-D does not provide any evidence for impurity (or more specifically: Ca) enhancement of densification rates.

An important caveat is that our model uses 10 year average [Ca] values, and therefore cannot resolve effects of inter-annual layering within the firn. Explicitly modeling the layering would require cm-scale resolution in the dynamical firn model, which is prohibitive from a computational point of view. Furthermore, [Ca] data at the required sub-annual resolution are difficult, if not impossible, to measure for the deepest part of the core where $\lambda(z)$ is below 1 cm a^{-1}. Increased firn layering and enhanced bulk densification affect the firn thickness in a similar manner; both lead to a shallower lock-in depth, and thereby a reduced $\delta^{15}N$. Therefore, in order to reconcile our WAIS-D results with the impurity-hypothesis of Horhold et al. (2012), one would need to invoke a strong reduction in LGM firn layering relative to the present day to compensate for the impurity-driven increase in bulk densification rates. However, recent work on the EDML core suggests that firn density layering was actually more pronounced during glacial times (Bendel et al., 2013). Including firn layering is therefore likely to only exacerbate the problem.

Work on present day firn has provided compelling arguments for a firn softening by impurity loading (Horhold et al., 2012; Freitag et al., 2013a, b). More work is needed to understand how densification rates are linked to impurity content in a mechanistic, rather than purely empirical way. Perhaps such a microscopic description could provide an explanation why firn densification rates at WAIS-D, to first order, do not appear to be affected by order-of-magnitude variations in [Ca] loading. One possible explanation

CPD
10, 3537–3584, 2014

could be that densification rates are controlled by some parameter that co-varies with Ca in modern day firn, yet does not change appreciably over glacial cycles.

4 Constructing the WAIS-Divide chronology

4.1 Annual layer count (0–31.2 ka)

A first layer counted chronology for the upper 2800 m of the WAIS-D core based on electrical conductivity measurements (ECM), named WDC06A-7, was presented by WAIS-Divide Project Members (2013). The WAIS chronology presented in this work, WD2014, uses an updated layer count for the upper 2850 m, based on new data and analyses that have become available since publication of WDC06A-7. These updates are:

1. A reassessment of the dating in the upper 577 m (2.4 ka) using high-resolution multi-parameter chemistry data in combination with automated layer detection algorithms (Winstrup et al., 2012);

2. A reassessment of the dating between 577–2300 m; (2.4–15.3 ka) using high resolution multi-parameter chemistry data in combination with ECM measurements;

3. A reassessment of the dating between 2300–2800 m; (15.3–29.5 ka) using ECM measurements in combination with high resolution multi-parameter chemistry data;

4. An extension of the annual layer dating between 2800–2850 m; (29.5–31.2 ka) using ECM measurements.

Details on the updated WAIS-D layer count and the layer counting methodology are presented in part 1 of the WD2014 papers (Sigl et al., 2014b).

CPD
10, 3537–3584, 2014

4.2 Methane synchronization (31.2–68 ka)

For the deep part of the core where an annual layer count is not available we date WAIS-D by synchronization to well-dated Northern Hemisphere (NH) climate records of abrupt DO variability using the WAIS-D record of globally well-mixed CH_4. This process consists of several steps:

1. Determine the midpoint of the abrupt DO transitions in WAIS-D CH_4, NGRIP $\delta^{18}O$ and Hulu speleothem $\delta^{18}O$.
2. Assign a gas age to the WAIS-D CH_4 tie-points (i.e., the DO transitions).
3. Apply the WAIS-D Δage (Sect. 3) to find the corresponding ice age at the depth of the CH_4 tie-points.
4. Interpolate between the ice age constraints to find the WAIS-D depth-age relationship.
5. Redo the Δage calculations on the new ice age scale.
6. Repeat steps 3–5 iteratively until the depth-age relationship is stable within 1 year. At WAIS-D this happened after 3 iterations.

These steps are described in more detail in the following sections.

4.3 Establishing the midpoint in abrupt DO transitions

The procedure for determining the midpoint of the abrupt DO warming transitions is depicted in Fig. 5. For each of the transitions we manually determine pre-event and post-event averages, as indicated by the orange lines. The averaging time is set to 150 and 50 years for stadial and interstadial periods, respectively; this difference in duration is used because (i) several of the interstadials are of short duration, and (ii) Greenland $\delta^{18}O$ is more variable during stadial climates, requiring longer averaging;

CPD
10, 3537–3584, 2014

in rare cases the duration of the pre-event stadial baseline climate was shorter than 150 years (such as for DO 16.1 at 58.33 ka BP), in which case the averaging time was shortened accordingly (Fig. 5).

After determining the pre- and post-event averages, we use linear interpolation of the timeseries to find the time at which the variable of interest had completed 25, 50 and 75 % of the total transition (Fig. 5). We use the 50 % marker (red) as the midpoint of the transition, which is used in the methane synchronization. The 25 % and 75 % markers (blue) are used as the $\pm 1\sigma$ uncertainty estimate. In rare cases the timeseries contain inversions within the transitions that lead to ambiguity in the timing of the markers; for these events we find the markers using a monotonic spline fit to the data.

The midpoints of abrupt interstadial terminations were determined in the same fashion (WAIS-D CH_4 and NGRIP only). Tables 1 and 2 give the results for NH warming, and NH cooling, respectively.

4.4 Synchronizing WAIS-D to a NGRIP-Hulu hybrid chronology

Abrupt DO variability is expressed clearly in a great number of NH climate records (Voelker, 2002). For the purpose of methane synchronization, our interest is in high-resolution records that express the abrupt DO events very clearly, and are furthermore exceptionally well dated. We here use a combination of two such NH records, namely the Greenland NGRIP δ^{18}O record (NGRIP community members, 2004), and a new version of the Hulu speleothem δ^{18}O record with improved resolution and additional dating constraints (see Wang et al., 2001, for a lower resolution Hulu δ^{18}O record). The DO events are resolved most clearly in the NGRIP δ^{18}O record, which is available at 20 year resolution. We use the GICC05-modelext chronology for this core, which is based on annual layer counting back to 60 ka BP, and on ice flow modeling for ice older than 60 ka (Rasmussen et al., 2006; Svensson et al., 2006; Wolff et al., 2010). While annual layer counting provides accurate relative ages (e.g., the duration of DO interstadials), it provides relatively inaccurate absolute ages due to the cumulative nature of counting uncertainty (Table 1). The updated Hulu δ^{18}O record also shows the abrupt

DO events in high temporal resolution (Fig. 5). The speleothem chronology is based on U/Th radiometric dating, providing much smaller uncertainty in the absolute ages than GICC05 (Table 1). The reason for selecting this record over other speleothem records is the large number of U/Th dates, the low detrital Th at the site, and the high sampling resolution of the δ^{18}O record (Wang et al., 2001). The onset of NH interstadial periods as expressed in Hulu δ^{18}O is given in Table 1.

A plot of the Hulu-NGRIP age difference is shown in Fig. 6, where the error bars denote the root sum square of the NGRIP and Hulu midpoint determination uncertainty (Sect. 4.3). The Hulu ages are systematically older than the NGRIP ages, and the age difference increases going further back in time. Note that the Hulu-NGRIP age difference is smaller than the stated GICC05 counting uncertainty (832 to 2573 years), but larger than the Hulu age uncertainty (92 to 366 years). A linear fit through these data, forced to intersect the origin, is given by 0.0063 × GICC05 age, suggesting that the GICC05 annual layer count on average misses only about 6 out of every 1000 layers. Because of this observation we use a linearly scaled version of GICC05 (GICC05 × 1.0063) as the target chronology for methane synchronization. This approach has several advantages. First, it respects both the superior relative ages (i.e., interval durations) of GICC05, as well as the superior absolute ages of the Hulu chronology. Second, it is very simple to convert between the WD2014 and GICC05 chronologies (CH_4-synchonized section of the chronology only); one simply needs to divide WD2014 ages by 1.0063 (and add 50 years to convert to the B2k reference date). Third, it still allows for direct synchronization of WAIS-D CH_4 to the NGRIP δ^{18}O record, providing more tie-points than direct synchronization to the Hulu record would.

The exercise of finding the transition midpoints and determining the GICC05-Hulu scaling factor was performed by two of the authors (J.P.S. and C.B.), independently of each other. The scaling factors obtained were 1.0063 and 1.0064, respectively, showing that, to first order, this result is insensitive to (subjective) judgment in identifying the transitions. The difference between the Hulu ages and 1.0063 × GICC05 ages are all within the stated Hulu 2σ dating error (Table 1). Consequently, our chronology is

CPD
10, 3537–3584, 2014

not in violation of any Hulu constraint as it respects the Hulu 2σ error at all of the tie points. In deriving the scaling we have assumed that the abrupt DO transitions observed in NGRIP and Hulu are simultaneous, which is not necessarily true. The variations in monsoon intensity represented by Hulu δ^{18}O are commonly explained by meridional movement of the inter tropical convergence zone (ITCZ) and tropical rainfall belts (Wang et al., 2001, 2006; Kanner et al., 2012); modeling work suggests such atmospheric readjustments occur on decadal timescales in response to NH high-latitude forcing (Chiang and Bitz, 2005; Broccoli et al., 2006; Cvijanovic and Chiang, 2013). Furthermore, CH_4 emissions, which are closely linked to tropical hydrology, change in phase with Greenland δ^{18}O, also suggesting that any time lags between NGRIP and Hulu are small (Huber et al., 2006; Baumgartner et al., 2014; Rosen et al., 2014). The uncertainty in the NGRIP-Hulu phasing is therefore small (decadal) relative to the correction we apply (up to 400 years).

Rather than synchronizing WAIS-D CH_4 to Greenland CH_4 records, we have chosen to synchronize directly to NGRIP δ^{18}O, which varies in phase with CH_4 (but with a more or less constant time lag). We let the midpoint in the CH_4 transitions lag the midpoint in the NGRIP δ^{18}O transition by 25 years, as suggested by studies of Greenland δ^{15}N-CH_4 phasing (Huber et al., 2006; Baumgartner et al., 2014; Rasmussen et al., 2013; Rosen et al., 2014). The rationale behind this approach is threefold. First, throughout MIS 3 the NGRIP δ^{18}O record has both better precision and higher temporal resolution than any available Greenland CH_4 record (Baumgartner et al., 2014; Brook et al., 1996; Blunier et al., 2007). Second, the dating of Greenland gas records depends on the highly variable Δage function, which is not equally well constrained for all DO events (Schwander et al., 1997; Rasmussen et al., 2013). This reliance on Greenland Δage would introduce an additional source of uncertainty. The best available Greenland CH_4 records are from NGRIP (Baumgartner et al., 2014) and NEEM (Chappellaz et al., 2013); for the former core no GICC05-based gas chronology exists to our knowledge (Kindler et al., 2014); for the latter core the gas chronology is based on the same assumption we use here, namely that the midpoint in the CH_4 transition lags the δ^{18}O

CPD
10, 3537–3584, 2014

transition by 25 years (Rasmussen et al., 2013). Third, Greenland CH_4 records should be more strongly impacted by firn smoothing than the WAIS-D CH_4 record, because glacial accumulation is lower in Greenland (Greenland glacial Δage is about 2–3 times as high as WAIS-D Δage during that time). In summary, our approach circumvents the uncertainties associated with using Greenland CH_4 as an intermediary.

4.5 Interpolation between age constraints

We can assign a gas age to each of the depths where an abrupt WAIS-D CH_4 transitions occurs; we do this for DO 4.1 through DO 18, i.e., the events prior to 31.2 ka BP (the onset of the WAIS-D layer count). The gas age we assign is equal to 1.0063 times the GICC05 age for the same event, with 25 years subtracted to account for the slight CH_4 lag behind Greenland δ^{18}O. By adding Δage (Sect. 3) to this gas age we assign an ice age. These assigned ages are printed in boldface in Tables 1 and 2.

To obtain a continuous depth-age relationship between these ice age constraints, we have to apply an interpolation strategy. This task amounts to estimating the annual layer thickness $\lambda(z)$ along the deep part of the core. The simplest approach is to assume a constant accumulation rate in between the age constraints; this is shown in Fig. 7b for the case where we use the age constraints from NH warming events only (black), or the age constraints from both NH warming and cooling events (red). The disadvantage of this approach is that it results in discontinuities in $\lambda(z)$ (the first derivative of the depth-age relationship), which we consider highly unrealistic. A more realistic approach is therefore to assume that $\lambda(z)$ is continuous and smooth (Fudge et al., 2014); Fig. 7b shows two scenarios in which we use a spline function to estimate $\lambda(z)$, where again we have applied age constraints from NH warming events only (orange) or age constraints from both NH warming and cooling events (blue).

For comparison, past A obtained from the firn densification model (Sect. 3) is plotted in green (Fig. 7b). While the δ^{15}N-based A follows the synchronization-based A estimates broadly, the millennial-scale details do not agree. We want to point out that this is not unexpected, since both methods have their imperfections. In particular, any

CPD
10, 3537–3584, 2014

errors in the GICC05 age model or in our modeled thinning function $f(z)$ will strongly impact the synchronization-based A estimates in Fig. 4.5b. The discrepancy is pronounced between 60–65 ka, where we have to strongly reduce $\lambda(z)$ in order to fit the age constraint(s) from DO 18, while δ^{15}N provides no evidence for very small A during this interval.

For the WD2014 chronology we have applied the smooth $\lambda(z)$ interpolation scheme using all age constraints (i.e., both NH warming and cooling events). The midpoint detection uncertainty is comparable for all events, and systematically smaller at the start of interstadial periods than at the terminations (Tables 1 and 2). For short interstadials (e.g., DO 9) this leads to a large relative uncertainty in the event duration, and thereby a large uncertainty in the implied accumulation rates (Fig. 7b). We force the interpolation to fit all NH warming constraints perfectly, yet relax this requirement for NH cooling constraints to prevent large swings in $\lambda(z)$ for the short duration events. The WD2014 chronology fits the NH warming and NH cooling age constraints with a 0 and 16 year root mean square offset, respectively.

4.6 Age uncertainty

The age uncertainty we assign to the deep part (> 2850 m) of the WD2014 chronology has four components.

The first source of uncertainty is the Δage calculation; we use the 2σ uncertainty obtained in the Δage sensitivity study (Sect. 3.2). The second source of uncertainty is the choice of interpolation scheme used to obtain a continuous chronology; here we use the standard deviation between the 4 different interpolation schemes of Fig. 7b) as an uncertainty estimate. The third source of uncertainty is the difficulty in determining the timing of the abrupt events in the timeseries; we use the uncertainty in the midpoint evaluation (root sum square of WAIS-D CH_4 and NGRIP δ^{18}O estimates). The last source of uncertainty is the age uncertainty in the hybrid NGRIP-Hulu chronology that we synchronize to. We use the stated Hulu age uncertainty, plus 50 years to account for possible leads or lags in the NGRIP-Hulu δ^{18}O phasing, plus the absolute value of the

CPD
10, 3537–3584, 2014

offset between the Hulu ages and the 1.0063 × GICC05 ages. For DO events where we do not have reliable Hulu age estimates (Table 1), we set the uncertainty to the Hulu age uncertainty of the nearest event, plus the uncertainty in the interval duration specified by the GICC05 layer count. For example, for DO 14 we do not have a reliable Hulu age estimate, and we use the Hulu age uncertainty of DO 16.2 (226 years) plus the uncertainty in the DO 14 to DO 16.2 interval duration on GICC05 (209 years), giving a total of 226 + 209 = 435 years.

The uncertainties (2σ values) are plotted in Fig. 7c (log scale). We assume these four uncertainties to be independent, and use their root sum square as the total uncertainty estimate on the WD2014 ice age scale (Fig. 7c, black curve). Note that the fourth source of uncertainty is only relevant when considering absolute ages; when evaluating relative ages (e.g., between WAIS-D ice and WAIS-D gas phase, or between WAIS-D and NGRIP) this last contribution does not need to be considered. For the deepest WAIS-D ice (3404 m depth) we thus find an age of 67.7 ± 0.9 ka BP.

5 Discussion

While the WAIS-Divide ice core does not extend as far back in time as deep cores from the East Antarctic plateau, it has the advantage of relatively high temporal resolution due to the high snow accumulation rate. WAIS-D accumulation rate during the LGM (~ 10 cm a^{-1} ice equivalent) is still higher than the present day accumulation rate at the EPICA (European project for ice coring in Antarctica) Dronning Maud Land core (7 cm a^{-1}), which is generally considered a high-accumulation core (EPICA Community Members, 2006). With 68 ka in 3404 m of core, the core average λ is 5 cm a^{-1}; at the onset of the last deglaciation (18 ka BP) λ is around 4 cm a^{-1}; near the bed λ is around 0.4 cm a^{-1}. This high temporal resolution provides the opportunity for obtaining very detailed climatic records.

High accumulation rates also result in a small Δage. Figure 8 compares Δage between several Antarctic cores (note the logarithmic scale). Δage at WAIS-D is approx-

CPD
10, 3537–3584, 2014

imately one third of the Δage at EPICA DML (EDML) and Talos Dome (TALDICE), and one tenth of the Δage at EPICA Dome C (EDC), Vostok and Dome Fuji. Because the uncertainty in the Δage (or Δdepth) calculation is typically on the order of ~ 20 %, a smaller Δage allows for a more precise inter-hemispheric synchronization with Greenland ice core records using CH_4. The small WAIS-D Δage uncertainty during MIS 3 allows investigation of the phasing of the bipolar seesaw (Stocker and Johnsen, 2003) at sub-centennial precision.

In comparing the shape of the Δage profiles, there are some interesting differences (Fig. 8). It is important to realize that not all the Δage histories shown were derived in the same way; WAIS-D and Dome Fuji Δage were derived using densification models, and the other four were derived using the Δdepth approach (Parrenin et al., 2012) and a Bayesian inverse method that includes a wide range of age markers (Veres et al., 2013). We will therefore compare the WAIS-D and Dome Fuji results. Δage at WAIS-D shows more pronounced variability than at Dome Fuji, particularly during MIS 3. The reason is that at Dome Fuji the glacial firn pack is about 4000 years old, and consequently the firn column integrates over 4000 years of climate variability, thereby dampening the Δage response to millennial scale climatic variability. At WAIS-D the glacial firn layer is only about 350 years old, and therefore the firn is in near-equilibrium with the millennial scale climate variations. This difference in response time is also obvious during the deglaciation, where WAIS-D Δage transitions from glacial to interglacial values between 18–14.5 ka BP, while Dome Fuji takes more time (18–10 ka BP). Surprisingly, EDML Δage does not show a strong deglacial Δage response, unlike all the other cores.

The relatively small Δage at WAIS-Divide also allows for precise investigation of the relative timing of atmospheric greenhouse gas variations and Antarctic climate (Barnola et al., 1991; Pedro et al., 2012; Caillon et al., 2003; Parrenin et al., 2013; Ahn et al., 2012). Recent work suggests that during the last deglaciation the rise in atmospheric CO_2 lagged the onset of pan-Antarctic warming by 0 to 400 years (Pedro et al., 2012; Parrenin et al., 2013). This Antarctic warming around 18 ka BP is

CPD
10, 3537–3584, 2014

presumably driven by the bipolar seesaw, as it coincides with a reduction in Atlantic overturning circulation strength as seen in North-Atlantic sediment records (McManus et al., 2004). The WAIS-D Δage at 18 ka (gas age) is 495 ± 75 years (2σ), much smaller than at central East-Antarctic sites such as EPICA Dome C, where Δage is approximately 3850 ± 900 years (Veres et al., 2013, with the Δage uncertainty taken to be the difference between the gas age and ice age uncertainties). The precision with which one can determine the relative phasing of climatic (i.e., $\delta^{18}O$ of ice) and atmospheric signals is set by the uncertainty in Δage (or equivalently, the uncertainty in Δdepth). Consequently, WAIS-D can make valuable contributions in investigating the phasing of greenhouse gas variations with Antarctic climate. However, the observation of asynchronous deglacial warming across the Antarctic continent (WAIS-Divide Project Members, 2013) suggests that attempts to capture the climate-CO_2 relationship in a single lead-lag value may be an oversimplification of deglacial climate dynamics.

An important next step will be to synchronize the WAIS-D chronology with other Antarctic cores via volcanic matching and other age markers (e.g., Severi et al., 2007; Sigl et al., 2014a). Because of the annual layer count and possibility of tight synchronization to Greenland ice cores, WAIS-D could contribute to an improved absolute dating of Antarctic cores, as well as improved cross-dating between cores. Such cross-dating could help inform the WAIS-D chronology as well, particularly in the deepest part of the core where the ice is potentially highly strained, as suggested by the interpolation difficulties in the 60–65 ka interval (Fig. 7b). With a synchronized chronology, WAIS-D could improve the representation of West-Antarctic climate in Antarctic ice core stacks (Pedro et al., 2011; Parrenin et al., 2013), and provide a more refined pan-Antarctic picture of the climate-CO_2 relationship.

6 Summary and conclusions

We have presented a first chronology for the deep (> 2850 m) section of the WAIS-Divide ice core, which is based on stratigraphic matching to Greenland ice cores using globally well-mixed methane. We use a dynamical firn densification model constrained by $\delta^{15}N$ data to calculate past Δage, and find that Δage was smaller than 525 ± 100 years for all of the core. The Δage reconstruction agrees well with values found using a recently developed Δdepth method that relies on ice flow modeling. Using high resolution WAIS-D records of atmospheric CH_4, we synchronize WAIS-D directly to Greenland NGRIP $\delta^{18}O$ for the abrupt onset and termination of each of the DO interstadials. To each event we assign an age corresponding to 1.0063 times its GICC05 age, which brings the ages in agreement with the high-resolution U/Th-dated Hulu speleothem record. The uncertainty in the final chronology is based on the uncertainties in: (i) the Δage calculations, as evaluated with a sensitivity study, (ii) the interpolation strategy, as evaluated by comparing four different interpolation methods, (iii) determining the timing of events in the different time series, and (iv) the ages of the hybrid NGRIP-Hulu chronology we are synchronizing to.

Due to the combination of a small Δage and a high-resolution methane record, the WAIS-Divide ice core can be synchronized more precisely to Greenland records than any other Antarctic core to date. This is important when investigating inter-hemispheric climate relationships such as the bipolar seesaw. The small WAIS-D Δage furthermore provides valuable opportunities for precise investigation of the relative phasing of atmospheric greenhouse gas variations and Antarctic climate.

Appendix A: Densification physics

A The densification rates used in this work are based on the empirical steady state model by Herron and Langway (1980) (the H-L model). We use the H-L model with minor modifications that allow it to be run dynamically (i.e., with time-variable T and A), and to include the softening effect of impurities following Freitag et al. (2013a). The H-L model divides the firn column in two stages, separated at the critical density $\rho_c = 550\,\mathrm{kg\,m^{-3}}$, occurring at the critical depth z_c.

CPD
10, 3537–3584, 2014

For the upper firn ($\rho \leq \rho_c$, stage 1), the densification rates are given by:

$$\frac{d\rho}{dt} = k_1 A (\rho_{ice} - \rho) \tag{A1}$$

with

$$k_1 = 11 \exp\left(-\frac{E_1}{RT}\right) \tag{A2}$$

where $E_1 = 10.16\,\mathrm{kJ\,mol^{-1}}$ is the activation energy for stage 1, and R the universal gas constant. Because both the sinking velocity of deposited layers ($w = dz/dt$) and the densification rate scale linearly with A, the resulting density-depth profile $\rho(z)$ in stage 1 becomes independent of A, and sensitive to T variations only.

For the deeper firn ($\rho > \rho_c$, stage 2), we use Eq. (4c) from Herron and Langway (1980), which was first derived by Sigfus J. Johnsen. This equation gives the densification rate in terms of overburden load, which allows the model to be run dynamically. The stage 2 densification rates are given by:

$$\frac{d\rho}{dt} = k_2^2 \frac{(\sigma_z - \sigma_{z_c})(\rho_{ice} - \rho)}{\ln\left[(\rho_{ice} - \rho_c)/(\rho_{ice} - \rho)\right]} \tag{A3}$$

with

$$k_2 = 575 \exp\left(-\frac{E_2}{RT}\right) \tag{A4}$$

where $E_2 = 21.4\,\mathrm{kJ\,mol^{-1}}$ is the activation energy for stage 2, and σ_z denotes the firn overburden load at a given depth in $\mathrm{Mg\,m^{-2}}$:

$$\sigma_z = \int_0^z \rho(z')dz'/1000 \tag{A5}$$

CPD
10, 3537–3584, 2014

Note that we divide by 1000 to convert from $\mathrm{kg\,m^{-3}}$ to $\mathrm{Mg\,m^{-3}}$, the units used by Herron and Langway (1980).

We use the mathematical description by Freitag et al. (2013a) to include the hypothesized firn softening effect of impurities. In this approach an increasing Ca concentration, as a proxy for mineral dust content, lowers the activation energy of firn, thereby enhancing densification rates. This is tantamount to stating that dusty firn behaves as if it were "warmer" than its climatological temperature. The H-L activation energies of Eqs. (A2) and (A4) are modified by [Ca] in the following way:

$$E^{\mathrm{Ca}} = E^{\mathrm{HL}} \times \alpha \left[1 - \beta \ln \left(\frac{[\mathrm{Ca}]}{[\mathrm{Ca}]_{\mathrm{crit}}} \right) \right] \tag{A6}$$

where E^{Ca} and E^{HL} are the Ca-modified and original H-L activation energies, respectively, $[\mathrm{Ca}]_{\mathrm{crit}} = 0.5\ \mu\mathrm{g\ kg^{-1}}$ is the minimum concentration at which impurities affect densification, and α and β are calibration parameters. Whenever $[\mathrm{Ca}](z) < [\mathrm{Ca}]_{\mathrm{crit}}$, we set $[\mathrm{Ca}](z) = [\mathrm{Ca}]_{\mathrm{crit}}$.

The parameter β sets the sensitivity to dust loading, and α is a normalization parameter that is included to account for the fact that the original H-L model was calibrated without the impurity effect. Consequently, if $\beta > 0$, one needs to compensate by setting $\alpha > 1$ to preserve the original H-L calibration. The work by Freitag et al. (2013a) recommends $\beta = 0.01$ and $\alpha = 1.025$ (which yields $E^{\mathrm{Ca}} = E^{\mathrm{HL}}$ at $[\mathrm{Ca}] = 5.73\,\mu\mathrm{g\,kg^{-1}}$).

In the experiment presented in Fig. 4 we changed the dust sensitivity β; it is clear that we need to simultaneously change α to keep the model well calibrated to present day conditions. To achieve this, we let $\alpha = 1.007 + \beta \ln(0.8/0.5)$ in the experiment, where we use the fact that the mean late Holocene [Ca] is around $0.8\,\mu\mathrm{g\ kg^{-1}}$ at WAIS-D. This approach ensures that, to first order, the present day E^{Ca} is invariant with β. This means that whatever value we choose for β, we will obtain a good fit to the present day Δage, δ^{15}N and A values that are are well known from direct observations (Battle et al., 2011).

CPD
10, 3537–3584, 2014

Acknowledgements. We thank Mark Twickler and Joseph Souney Jr. of the WAIS Divide Science Coordination Office, the Ice Drilling Design and Operations group at the University of Wisconsin for recovering the ice core, O. Maselli, N. Chellman, M. Grieman, J. D'Andrilli, L. Layman, and R. Grinstead for help in making the continuous CH_4 and Ca measurements, Raytheon Polar Services for logistics support in Antarctica, the 109th New York Air National Guard for airlift in Antarctica, Dan Muhs for useful feedback on the manuscript, and the dozens of core handlers in the field and at the National Ice Core Laboratory for the core processing. This work is funded by the US National Science Foundation through grants 0539232, 0537661 (to K. M. C.), ANT05-38657 (to J. P. S.), NSFC 41230524 (to H. C. and R. L. E), 0839093, 1142166 (to J. R. M.) 1043092 (to E. J. S.) and through grants 0230396, 0440817, 0944348 and 0944266 to the Desert Research Institute of Reno Nevada and University of New Hampshire for the collection and distribution of the WAIS Divide ice core and related tasks. We further acknowledge support by the NOAA Climate and Global Change fellowship program, administered by the University Corporation for Atmospheric Research (to C. B.).

References

Aciego, S., Bourdon, B., Schwander, J., Baur, H., and Forieri, A.: Toward a radiometric ice clock: uranium ages of the Dome C ice core, Quaternary Sci. Rev., 30, 2389–2397, doi:10.1016/j.quascirev.2011.06.008, 2011. 3541

Ahn, J. and Brook, E. J.: Atmospheric CO_2 and climate on millennial time scales during the last glacial period, Science, 322, 83–85, doi:10.1126/science.1160832, 2008. 3539

Ahn, J., Brook, E. J., Schmittner, A., and Kreutz, K.: Abrupt change in atmospheric CO_2 during the last ice age, Geophys. Res. Lett., 39, L18711, doi:10.1029/2012gl053018, 2012. 3559

Barnola, J. M., Pimienta, P., Raynaud, D., and Korotkevich, Y. S.: CO_2-climate relationship as deduced from the Vostok ice core: a re-examination based on new measurements and on a re-evaluation of the air dating, Tellus B., 43, 83–90, 1991. 3543, 3559

Battle, M. O., Severinghaus, J. P., Sofen, E. D., Plotkin, D., Orsi, A. J., Aydin, M., Montzka, S. A., Sowers, T., and Tans, P. P.: Controls on the movement and composition of firn air at the West Antarctic Ice Sheet Divide, Atmos. Chem. Phys., 11, 11007–11021, doi:10.5194/acp-11-11007-2011, 2011. 3547, 3563

Baumgartner, M., Kindler, P., Eicher, O., Floch, G., Schilt, A., Schwander, J., Spahni, R., Capron, E., Chappellaz, J., Leuenberger, M., Fischer, H., and Stocker, T. F.: NGRIP CH_4 concentration from 120 to 10 kyr before present and its relation to a δ^{15}N temperature reconstruction from the same ice core, Clim. Past, 10, 903–920, doi:10.5194/cp-10-903-2014, 2014. 3555

Bazin, L., Landais, A., Lemieux-Dudon, B., Toyé Mahamadou Kele, H., Veres, D., Parrenin, F., Martinerie, P., Ritz, C., Capron, E., Lipenkov, V., Loutre, M.-F., Raynaud, D., Vinther, B., Svensson, A., Rasmussen, S. O., Severi, M., Blunier, T., Leuenberger, M., Fischer, H., Masson-Delmotte, V., Chappellaz, J., and Wolff, E.: An optimized multi-proxy, multi-site Antarctic ice and gas orbital chronology (AICC2012): 120–800 ka, Clim. Past, 9, 1715–1731, doi:10.5194/cp-9-1715-2013, 2013. 3584

Bendel, V., Ueltzhoffer, K. J., Freitag, J., Kipfstuhl, S., Kuhs, W. F., Garbe, C. S., and Faria, S. H.: High-resolution variations in size, number and arrangement of air bubbles in the EPICA DML (Antarctica) ice core, J. Glaciol., 59, 972–980, 2013. 3550

Bender, M. L.: Orbital tuning chronology for the Vostok climate record supported by trapped gas composition, Earth Planet. Sc. Lett., 204, 275–289, 2002. 3540

Bender, M. L., Barnett, B., Dreyfus, G., Jouzel, J., and Porcelli, D.: The contemporary degassing rate of Ar-40 from the Solid Earth, P. Natl. Acad. Sci. USA, 105, 8232–8237, doi:10.1073/pnas.0711679105, 2008. 3541

Blunier, T. and Brook, E. J.: Timing of millennial-scale climate change in Antarctica and Greenland during the last glacial period, Science, 291, 109–112, 2001. 3541

Blunier, T. and Schwander, J.: Gas enclosure in ice: age difference and fractionation, in: Physics of Ice Core Records, edited by: Hondoh, T., Hokkaido University Press, Sapporo, 307–326, 2000. 3544

Blunier, T., Chappellaz, J., Schwander, J., Dallenbach, A., Stauffer, B., Stocker, T. F., Raynaud, D., Jouzel, J., Clausen, H. B., Hammer, C. U., and Johnsen, S. J.: Asynchrony of Antarctic and Greenland climate change during the last glacial period, Nature, 394, 739–743, doi:10.1038/29447, 1998. 3541

Blunier, T., Spahni, R., Barnola, J.-M., Chappellaz, J., Loulergue, L., and Schwander, J.: Synchronization of ice core records via atmospheric gases, Clim. Past, 3, 325–330, doi:10.5194/cp-3-325-2007, 2007. 3541, 3555

Broccoli, A. J., Dahl, K. A., and Stouffer, R. J.: Response of the ITCZ to Northern Hemisphere cooling, Geophys. Res. Lett., 33, L01702, doi:10.1029/2005gl024546, 2006. 3555

Brook, E. J., Sowers, T., and Orchardo, J.: Rapid variations in atmospheric methane concentration during the past 110,000 years, Science, 273, 1087–1091, 1996. 3555

Buizert, C., Martinerie, P., Petrenko, V. V., Severinghaus, J. P., Trudinger, C. M., Witrant, E., Rosen, J. L., Orsi, A. J., Rubino, M., Etheridge, D. M., Steele, L. P., Hogan, C., Laube, J. C., Sturges, W. T., Levchenko, V. A., Smith, A. M., Levin, I., Conway, T. J., Dlugokencky, E. J., Lang, P. M., Kawamura, K., Jenk, T. M., White, J. W. C., Sowers, T., Schwander, J., and Blunier, T.: Gas transport in firn: multiple-tracer characterisation and model intercomparison for NEEM, Northern Greenland, Atmos. Chem. Phys., 12, 4259–4277, doi:10.5194/acp-12-4259-2012, 2012. 3544

Buizert, C., Sowers, T., and Blunier, T.: Assessment of diffusive isotopic fractionation in polar firn, and application to ice core trace gas records, Earth Planet. Sc. Lett., 361, 110–119, doi:10.1016/j.epsl.2012.11.039, 2013. 3544

Buizert, C., Baggenstos, D., Jiang, W., Purtschert, R., Petrenko, V. V., Lu, Z.-T., Muller, P., Kuhl, T., Lee, J., Severinghaus, J. P., and Brook, E. J.: Radiometric ^{81}Kr dating identifies 120,000-year-old ice at Taylor Glacier, Antarctica, P. Natl. Acad. Sci. USA, 111, 6876–6881, doi:10.1073/pnas.1320329111, 2014. 3541

Caillon, N., Severinghaus, J. P., Jouzel, J., Barnola, J.-M., Kang, J., and Lipenkov, V. Y.: Timing of atmospheric CO_2 and antarctic temperature changes across termination III, Science, 299, 1728–1731, doi:10.1126/science.1078758, 2003. 3559

Capron, E., Landais, A., Chappellaz, J., Schilt, A., Buiron, D., Dahl-Jensen, D., Johnsen, S. J., Jouzel, J., Lemieux-Dudon, B., Loulergue, L., Leuenberger, M., Masson-Delmotte, V., Meyer, H., Oerter, H., and Stenni, B.: Millennial and sub-millennial scale climatic variations recorded in polar ice cores over the last glacial period, Clim. Past, 6, 345–365, doi:10.5194/cp-6-345-2010, 2010. 3541

Chappellaz, J., Stowasser, C., Blunier, T., Baslev-Clausen, D., Brook, E. J., Dallmayr, R., Faïn, X., Lee, J. E., Mitchell, L. E., Pascual, O., Romanini, D., Rosen, J., and Schüpbach, S.: High-resolution glacial and deglacial record of atmospheric methane by continuous-flow and laser spectrometer analysis along the NEEM ice core, Clim. Past, 9, 2579–2593, doi:10.5194/cp-9-2579-2013, 2013. 3555

Chiang, J. C. H. and Bitz, C. M.: Influence of high latitude ice cover on the marine Intertropical Convergence Zone, Clim. Dynam., 25, 477–496, doi:10.1007/s00382-005-0040-5, 2005. 3555

Cuffey, K. M. and Clow, G. D.: Temperature, accumulation, and ice sheet elevation in central Greenland through the last deglacial transition, J. Geophys. Res., 102, 26383–26396, doi:10.1029/96jc03981, 1997. 3544

Cuffey, K. M. and Paterson, W. S. B.: The Physics of Glaciers, 4th edn., Butterworth-Heinemann, Oxford, UK, 2010. 3544, 3545

Cuffey, K. M., Clow, G. D., Alley, R. B., Stuiver, M., Waddington, E. D., and Saltus, R. W.: Large arctic temperature change at the Wisconsin-Holocene glacial transition, Science, 270, 455–458, 1995. 3544

Cuffey, K. M. et al.: in preparation, 2014. 3545

Cvijanovic, I. and Chiang, J. C. H.: Global energy budget changes to high latitude North Atlantic cooling and the tropical ITCZ response, Clim. Dynam., 40, 1435–1452, doi:10.1007/s00382-012-1482-1, 2013. 3555

Dahl-Jensen, D., Mosegaard, K., Gundestrup, N., Clow, G. D., Johnsen, S. J., Hansen, A. W., and Balling, N.: Past temperatures directly from the greenland ice sheet, Science, 282, 268–271, doi:10.1126/science.282.5387.268, 1998. 3540

Dlugokencky, E., Myers, R., Lang, P., Masarie, K., Crotwell, A., Thoning, K., Hall, B., Elkins, J., and Steele, L.: Conversion of NOAA atmospheric dry air CH_4 mole fractions to a gravimetrically prepared standard scale, J. Geophys. Res.-Atmos., 110, D18306, doi:10.1029/2005JD006035, 2005. 3542

Dreyfus, G. B., Jouzel, J., Bender, M. L., Landais, A., Masson-Delmotte, V., and Leuenberger, M.: Firn processes and δ^{15}N: potential for a gas-phase climate proxy, Quaternary Sci. Rev., 29, 28–42, 2010. 3547

EPICA Community Members: One-to-one coupling of glacial climate variability in Greenland and Antarctica, Nature, 444, 195–198, doi:10.1038/nature05301, 2006. 3539, 3558

Etheridge, D. M., Pearman, G. I., and Fraser, P. J.: Changes in tropospheric methane between 1841 and 1978 from a high accumulation-rate Antarctic ice core, Tellus B, 44, 282–294, doi:10.1034/j.1600-0889.1992.t01-3-00006.x, 1992. 3548

Freitag, J., Kipfstuhl, J., Laepple, T., and Wilhelms, F.: Impurity-controlled densification: a new model for stratified polar firn, J. Glaciol., 59, 1163–1169, 2013a. 3544, 3548, 3549, 3550, 3561, 3563

Freitag, J., Kipfstuhl, S., and Laepple, T.: Core-scale radioscopic imaging: a new method reveals density-calcium link in Antarctic firn, J. Glaciol., 59, 1009–1014, 2013b. 3550

CPD
10, 3537–3584, 2014

Fudge, T. J., Waddington, E. D., Conway, H., Lundin, J. M. D., and Taylor, K.: Interpolation methods for Antarctic ice-core timescales: application to Byrd, Siple Dome and Law Dome ice cores, Clim. Past, 10, 1195–1209, doi:10.5194/cp-10-1195-2014, 2014. 3556

Goujon, C., Barnola, J. M., and Ritz, C.: Modeling the densification of polar firn including heat diffusion: Application to close-off characteristics and gas isotopic fractionation for Antarctica and Greenland sites, J. Geophys. Res.-Atmos., 108, 18, doi:10.1029/2002jd003319, 2003. 3543

Gow, A. J., Meese, D. A., Alley, R. B., Fitzpatrick, J. J., Anandakrishnan, S., Woods, G. A., and Elder, B. C.: Physical and structural properties of the Greenland Ice Sheet Project 2 ice core: a review, J. Geophys. Res.-Oceans, 102, 26559–26575, doi:10.1029/97JC00165, 1997. 3540

Gundestrup, N. S., Dahl-Jensen, D., Hansen, B. L., and Kelty, J.: Bore-hole survey at Camp Century, 1989, Cold Reg. Sci. Technol., 21, 187–193, doi:10.1016/0165-232x(93)90006-t, 1993. 3539

Herron, M. M. and Langway, C. C.: Firn densification: an empirical model, J. Glaciol., 25, 373–385, 1980. 3543, 3544, 3547, 3561, 3562, 3563

Horhold, M. W., Laepple, T., Freitag, J., Bigler, M., Fischer, H., and Kipfstuhl, S.: On the impact of impurities on the densification of polar firn, Earth Planet. Sc. Lett., 325–326, 93–99, doi:10.1016/j.epsl.2011.12.022, 2012. 3544, 3548, 3549, 3550

Huber, C., Leuenberger, M., Spahni, R., Fluckiger, J., Schwander, J., Stocker, T. F., Johnsen, S., Landals, A., and Jouzel, J.: Isotope calibrated Greenland temperature record over Marine Isotope Stage 3 and its relation to CH_4, Earth Planet. Sc. Lett., 243, 504–519, doi:10.1016/j.epsl.2006.01.002, 2006. 3555

Johnsen, S. J., Dahl-Jensen, D., Gundestrup, N., Steffensen, J. P., Clausen, H. B., Miller, H., Masson-Delmotte, V., Sveinbjörnsdottir, A. E., and White, J.: Oxygen isotope and palaeotemperature records from six Greenland ice-core stations: Camp Century, Dye-3, GRIP, GISP2, Renland and NorthGRIP, J. Quaternary Sci., 16, 299–307, doi:10.1002/jqs.622, 2001. 3540

Kanner, L. C., Burns, S. J., Cheng, H., and Edwards, R. L.: High-latitude forcing of the south American summer monsoon during the last glacial, Science, 335, 570–573, 2012. 3555

Kaspers, K. A., van de Wal, R. S. W., van den Broeke, M. R., Schwander, J., van Lipzig, N. P. M., and Brenninkmeijer, C. A. M.: Model calculations of the age of firn air across the Antarctic continent, Atmos. Chem. Phys., 4, 1365–1380, doi:10.5194/acp-4-1365-2004, 2004. 3547, 3548

Kawamura, K., Severinghaus, J. P., Ishidoya, S., Sugawara, S., Hashida, G., Motoyama, H., Fujii, Y., Aoki, S., and Nakazawa, T.: Convective mixing of air in firn at four polar sites, Earth Planet. Sc. Lett., 244, 672–682, 2006. 3547

Kawamura, K., Parrenin, F., Lisiecki, L., Uemura, R., Vimeux, F., Severinghaus, J. P., Hutterli, M. A., Nakazawa, T., Aoki, S., Jouzel, J., Raymo, M. E., Matsumoto, K., Nakata, H., Motoyama, H., Fujita, S., Goto-Azuma, K., Fujii, Y., and Watanabe, O.: Northern Hemisphere forcing of climatic cycles in Antarctica over the past 360,000 years, Nature, 448, 912–916, doi:10.1038/nature06015, 2007. 3540, 3584

Kindler, P., Guillevic, M., Baumgartner, M., Schwander, J., Landais, A., and Leuenberger, M.: Temperature reconstruction from 10 to 120 kyr b2k from the NGRIP ice core, Clim. Past, 10, 887–902, doi:10.5194/cp-10-887-2014, 2014. 3555

Lal, D., Jull, A. J. T., Donahue, D. J., Burtner, D., and Nishiizumi, K.: Polar ice ablation rates measured using in situ cosmogenic C-14, Nature, 346, 350–352, 1990. 3541

Landais, A., Barnola, J. M., Kawamura, K., Caillon, N., Delmotte, M., Van Ommen, T., Dreyfus, G., Jouzel, J., Masson-Delmotte, V., Minster, B., Freitag, J., Leuenberger, M., Schwander, J., Huber, C., Etheridge, D., and Morgan, V.: Firn-air delta N-15 in modern polar sites and glacial-interglacial ice: a model-data mismatch during glacial periods in Antarctica?, Quaternary Sci. Rev., 25, 49–62, doi:10.1016/j.quascirev.2005.06.007, 2006. 3545

Martinerie, P., Lipenkov, V. Y., Raynaud, D., Chappellaz, J., Barkov, N. I., and Lorius, C.: Air content paleo record in the Vostok ice core (Antarctica): A mixed record of climatic and glaciological parameters, J. Geophys. Res.-Atmos., 99, 10565–10576, 1994. 3544

McConnell, J. R., Lamorey, G. W., Lambert, S. W., and Taylor, K. C.: Continuous ice-core chemical analyses using inductively coupled plasma mass spectrometry, Environ. Sci. Technol., 36, 7–11, doi:10.1021/es011088z, 2002. 3543

McConnell, J. R., Edwards, R., Kok, G. L., Flanner, M. G., Zender, C. S., Saltzman, E. S., Banta, J. R., Pasteris, D. R., Carter, M. M., and Kahl, J. D. W.: 20th-century industrial black carbon emissions altered arctic climate forcing, Science, 317, 1381–1384, doi:10.1126/science.1144856, 2007. 3543

McManus, J. F., Francois, R., Gherardi, J. M., Keigwin, L. D., and Brown-Leger, S.: Collapse and rapid resumption of Atlantic meridional circulation linked to deglacial climate changes, Nature, 428, 834–837, doi:10.1038/nature02494, 2004. 3560

Mischler, J. A., Sowers, T. A., Alley, R. B., Battle, M., McConnell, J. R., Mitchell, L., Popp, T., Sofen, E., and Spencer, M. K.: Carbon and hydrogen isotopic composition of methane

CPD
10, 3537–3584, 2014
The WAIS-Divide chronology – Part 2: Methane synchronization
C. Buizert et al.

over the last 1000 years, Global Biogeochem. Cy., 23, GB4024, doi:10.1029/2009gb003460, 2009. 3540
Mitchell, L., Brook, E., Lee, J. E., Buizert, C., and Sowers, T.: Constraints on the late holocene anthropogenic contribution to the atmospheric methane budget, Science, 342, 964–966, doi:10.1126/science.1238920, 2013. 3540
Mitchell, L. E., Brook, E. J., Sowers, T., McConnell, J. R., and Taylor, K.: Multidecadal variability of atmospheric methane, 1000–1800 C.E, J. Geophys. Res., 116, G02007, doi:10.1029/2010jg001441, 2011. 3540, 3542
NEEM community members: Eemian interglacial reconstructed from a Greenland folded ice core, Nature, 493, 489–494, 2013. 3539
NGRIP community members: High-resolution record of Northern Hemisphere climate extending into the last interglacial period, Nature, 431, 147–151, doi:10.1038/nature02805, 2004. 3539, 3553
Orsi, A. J.: Temperature reconstruction at the West Antarctic Ice Sheet Divide, for the last millennium, from the combination of borehole temperature and inert gas isotope measurements, Ph. D. thesis, University of California, San Diego, 2013. 3548
Parrenin, F., Barker, S., Blunier, T., Chappellaz, J., Jouzel, J., Landais, A., Masson-Delmotte, V., Schwander, J., and Veres, D.: On the gas-ice depth difference (Δdepth) along the EPICA Dome C ice core, Clim. Past, 8, 1239–1255, doi:10.5194/cp-8-1239-2012, 2012. 3546, 3550, 3559
Parrenin, F., Masson-Delmotte, V., Kohler, P., Raynaud, D., Paillard, D., Schwander, J., Barbante, C., Landais, A., Wegner, A., and Jouzel, J.: Synchronous change of atmospheric CO_2 and antarctic temperature during the last deglacial warming, Science, 339, 1060–1063, doi:10.1126/science.1226368, 2013. 3559, 3560
Pedro, J. B., van Ommen, T. D., Rasmussen, S. O., Morgan, V. I., Chappellaz, J., Moy, A. D., Masson-Delmotte, V., and Delmotte, M.: The last deglaciation: timing the bipolar seesaw, Clim. Past, 7, 671–683, doi:10.5194/cp-7-671-2011, 2011. 3560
Pedro, J. B., Rasmussen, S. O., and van Ommen, T. D.: Tightened constraints on the time-lag between Antarctic temperature and CO_2 during the last deglaciation, Clim. Past, 8, 1213–1221, doi:10.5194/cp-8-1213-2012, 2012. 3559
Petrenko, V. V., Severinghaus, J. P., Brook, E. J., Reeh, N., and Schaefer, H.: Gas records from the West Greenland ice margin covering the Last Glacial Termination: a horizontal ice core, Quaternary Sci. Rev., 25, 865–875, 2006. 3541, 3543

Rasmussen, S. O., Andersen, K. K., Svensson, A. M., Steffensen, J. P., Vinther, B. M., Clausen, H. B., Siggaard-Andersen, M. L., Johnsen, S. J., Larsen, L. B., Dahl-Jensen, D., Bigler, M., Röthlisberger, R., Fischer, H., Goto-Azuma, K., Hansson, M. E., and Ruth, U.: A new Greenland ice core chronology for the last glacial termination, J. Geophys. Res., 111, D06102, doi:10.1029/2005jd006079, 2006. 3553

Rasmussen, S. O., Abbott, P. M., Blunier, T., Bourne, A. J., Brook, E., Buchardt, S. L., Buizert, C., Chappellaz, J., Clausen, H. B., Cook, E., Dahl-Jensen, D., Davies, S. M., Guillevic, M., Kipfstuhl, S., Laepple, T., Seierstad, I. K., Severinghaus, J. P., Steffensen, J. P., Stowasser, C., Svensson, A., Vallelonga, P., Vinther, B. M., Wilhelms, F., and Winstrup, M.: A first chronology for the North Greenland Eemian Ice Drilling (NEEM) ice core, Clim. Past, 9, 2713–2730, doi:10.5194/cp-9-2713-2013, 2013. 3543, 3555, 3556

Rhodes, R. H., Fain, X., Stowasser, C., Blunier, T., Chappellaz, J., McConnell, J. R., Romanini, D., Mitchell, L. E., and Brook, E. J.: Continuous methane measurements from a late Holocene Greenland ice core: atmospheric and in-situ signals, Earth Planet. Sc. Lett., 368, 9–19, doi:10.1016/j.epsl.2013.02.034, 2013. 3542, 3548

Rhodes, R. H. et al.: in preparation, 2014. 3542

Rosen, J. L., Brook, E. J., Severinghaus, J. P., Blunier, T., Mitchell, L. E., Lee, J. E., Edwards, J. S., and Gkinis, V.: An ice core record of near-synchronous global climate changes at the Bolling transition, Nat. Geosci., 7, 459–463, 2014. 3555

Schwander, J. and Stauffer, B.: Age difference between polar ice and the air trapped in its bubbles, Nature, 311, 45–47, 1984. 3543

Schwander, J., Sowers, T., Barnola, J. M., Blunier, T., Fuchs, A., and Malaize, B.: Age scale of the air in the summit ice: Implication for glacial-interglacial temperature change, J. Geophys. Res.-Atmos., 102, 19483–19493, 1997. 3543, 3555

Seierstad, I., Abbott, P., Bigler, M., Blunier, T., Bourne, A., Brook, E., Buchardt, S. L., Buizert, C., Clausen, H. B., Cook, E., Dahl-Jensen, D., Davies, S., Guillevic, M., Johnsen, S., Pedersen, D., Popp, T., Rasmussen, S. O., Severinghaus, J., Svensson, A., and Vinther, B.: Consistently dated records from the Greenland GRIP, GISP2 and NGRIP ice cores for the past 104 ka reveal regional millennial-scale isotope gradients with possible Heinrich Event imprint, Quaternary Sci. Rev., in review, 2014. 3543

Severi, M., Becagli, S., Castellano, E., Morganti, A., Traversi, R., Udisti, R., Ruth, U., Fischer, H., Huybrechts, P., Wolff, E., Parrenin, F., Kaufmann, P., Lambert, F., and Steffensen, J. P.: Syn-

CPD
10, 3537–3584, 2014

chronisation of the EDML and EDC ice cores for the last 52 kyr by volcanic signature matching, Clim. Past, 3, 367–374, doi:10.5194/cp-3-367-2007, 2007. 3560

Severinghaus, J. P., Beaudette, R., Headly, M. A., Taylor, K., and Brook, E. J.: Oxygen-18 of O_2 records the impact of abrupt climate change on the terrestrial biosphere, Science, 324, 1431–1434, doi:10.1126/science.1169473, 2009. 3543

Sigl, M., McConnell, J. R., Layman, L., Maselli, O., McGwire, K., Pasteris, D., Dahl-Jensen, D., Steffensen, J. P., Vinther, B., Edwards, R., Mulvaney, R., and Kipfstuhl, S.: A new bipolar ice core record of volcanism from WAIS Divide and NEEM and implications for climate forcing of the last 2000 years, J. Geophys. Res.-Atmos., 118, 1151–1169, doi:10.1029/2012JD018603, 2013. 3540

Sigl, M., McConnell, J. R., Toohey, M., Curran, M., Das, S. B., Edwards, R., Isaksson, E., Kawamura, K., Kipfstuhl, S., Krüger, K., Layman, L., Maselli, O. J., Motizuki, Y., Motoyama, H., Pasteris, D. R., and Severi, M.: Insights from Antarctica on volcanic forcing during the Common Era, Nature Climate Change, 4, 693–697, doi:10.1038/nclimate2293, 2014. 3560

Sigl, M. et al.: in preparation, 2014. 3541, 3551

Sowers, T., Bender, M., and Raynaud, D.: Elemental and isotopic composition of occluded O_2 and N_2 in polar ice, J. Geophys. Res.-Atmos., 94, 5137–5150, doi:10.1029/JD094iD04p05137, 1989. 3543

Sowers, T., Bender, M., Raynaud, D., and Korotkevich, Y. S.: $\delta^{15}N$ of N_2 in air trapped in polar ice: A tracer of gas transport in the firn and a possible constraint on ice age-gas age differences, J. Geophys. Res.-Atmos., 97, 15683–15697, 1992. 3543, 3547

Steig, E. J., Ding, Q., White, J. W. C., Kuttel, M., Rupper, S. B., Neumann, T. A., Neff, P. D., Gallant, A. J. E., Mayewski, P. A., Taylor, K. C., Hoffmann, G., Dixon, D. A., Schoenemann, S. W., Markle, B. R., Fudge, T. J., Schneider, D. P., Schauer, A. J., Teel, R. P., Vaughn, B. H., Burgener, L., Williams, J., and Korotkikh, E.: Recent climate and ice-sheet changes in West Antarctica compared with the past 2,000 years, Nat. Geosci., 6, 372–375, doi:10.1038/ngeo1778, 2013. 3540, 3542

Stocker, T. F. and Johnsen, S. J.: A minimum thermodynamic model for the bipolar seesaw, Paleoceanography, 18, 1087, doi:10.1029/2003pa000920, 2003. 3559

Stowasser, C., Buizert, C., Gkinis, V., Chappellaz, J., Schüpbach, S., Bigler, M., Faïn, X., Sperlich, P., Baumgartner, M., Schilt, A., and Blunier, T.: Continuous measurements of methane mixing ratios from ice cores, Atmos. Meas. Tech., 5, 999–1013, doi:10.5194/amt-5-999-2012, 2012. 3542

Svensson, A., Andersen, K. K., Bigler, M., Clausen, H. B., Dahl-Jensen, D., Davies, S. M., Johnsen, S. J., Muscheler, R., Rasmussen, S. O., Rothlisberger, R., Steffensen, J. P., and Vinther, B. M.: The Greenland Ice Core Chronology 2005, 15–42 ka. Part 2: Comparison to other records, Quaternary Sci. Rev., 25, 3258–3267, doi:10.1016/j.quascirev.2006.08.003, 2006. 3553

Veres, D., Bazin, L., Landais, A., Toyé Mahamadou Kele, H., Lemieux-Dudon, B., Parrenin, F., Martinerie, P., Blayo, E., Blunier, T., Capron, E., Chappellaz, J., Rasmussen, S. O., Severi, M., Svensson, A., Vinther, B., and Wolff, E. W.: The Antarctic ice core chronology (AICC2012): an optimized multi-parameter and multi-site dating approach for the last 120 thousand years, Clim. Past, 9, 1733–1748, doi:10.5194/cp-9-1733-2013, 2013. 3559, 3560, 3584

Voelker, A. H. L.: Global distribution of centennial-scale records for Marine Isotope Stage (MIS) 3: A database, Quaternary Sci. Rev., 21, 1185–1212, doi:10.1016/s0277-3791(01)00139-1, 2002. 3553

WAIS-Divide Project Members: Onset of deglacial warming in West Antarctica driven by local orbital forcing, Nature, 500, 440–444, doi:10.1038/nature12376, 2013. 3540, 3541, 3542, 3544, 3546, 3551, 3560

Wang, X. F., Auler, A. S., Edwards, R. L., Cheng, H., Ito, E., and Solheid, M.: Interhemispheric anti-phasing of rainfall during the last glacial period, Quaternary Sci. Rev., 25, 3391–3403, doi:10.1016/j.quascirev.2006.02.009, 2006. 3555

Wang, Y. J., Cheng, H., Edwards, R. L., An, Z. S., Wu, J. Y., Shen, C. C., and Dorale, J. A.: A high-resolution absolute-dated late pleistocene monsoon record from Hulu Cave, China, Science, 294, 2345–2348, 2001. 3553, 3554, 3555

Winstrup, M., Svensson, A. M., Rasmussen, S. O., Winther, O., Steig, E. J., and Axelrod, A. E.: An automated approach for annual layer counting in ice cores, Clim. Past, 8, 1881–1895, doi:10.5194/cp-8-1881-2012, 2012. 3551

Wolff, E. W., Fischer, H., Fundel, F., Ruth, U., Twarloh, B., Littot, G. C., Mulvaney, R., Rothlisberger, R., de Angelis, M., Boutron, C. F., Hansson, M., Jonsell, U., Hutterli, M. A., Lambert, F., Kaufmann, P., Stauffer, B., Stocker, T. F., Steffensen, J. P., Bigler, M., Siggaard-Andersen, M. L., Udisti, R., Becagli, S., Castellano, E., Severi, M., Wagenbach, D., Barbante, C., Gabrielli, P., and Gaspari, V.: Southern Ocean sea-ice extent, productivity and iron flux over the past eight glacial cycles, Nature, 440, 491–496, 2006. 3539

CPD

10, 3537–3584, 2014

The WAIS-Divide chronology – Part 2: Methane synchronization

C. Buizert et al.

Wolff, E. W., Chappellaz, J., Blunier, T., Rasmussen, S. O., and Svensson, A.: Millennial-scale variability during the last glacial: the ice core record, Quaternary Sci. Rev., 29, 2828–2838, 2010. 3540, 3553

CPD
10, 3537–3584, 2014

Table 1. Overview of CH_4 tiepoints for NH warming events.

	NGRIP				Hulu			WAIS-D			
	Depth (m)	Age (year bp)	Age uncert. (year)	Midpoint (year)	Hulu age (year bp)	Age uncert. (year)	Midpoint (year)	Depth (m)	Gas age (year bp)	Ice age (year bp)	Midpoint (year)
YD-PB	1490.89	11 619	98	23				1983.02	11 542	11 740	33
OD-YD	1604.05	14 628	185	15				2259.39	14 576	14 804	29
DO 2	1793.51	23 303	597	16				2632.08	23 988	24 467	30
DO 3	1869.00	27 728	832	12	27 922	95	39	2755.74	27 749	28 144	19
DO 4	1891.27	28 838	898	14	29 134	92	21	2797.92	28 993	29 397	23
DO 5.1	1919.48	30 731	1023	11	30 876	255	37	2848.36	30 735	31 185	22
DO 5.2	1951.66	32 452	1132	15	32 667	236	21	2885.44	**32 631**	**33 028**	17
DO 6	1974.48	33 687	1213	19	34 034	337	36	2913.01	**33 874**	**34 270**	18
DO 7	2009.62	35 437	1321	16	35 532	299	20	2958.64	**35 636**	**35 979**	20
DO 8	2069.88	38 165	1449	13	38 307	155	19	3021.37	**38 381**	**38 674**	33
DO 9	2099.50	40 104	1580	13	40 264	241	42	3066.52	**40 332**	**40 681**	19
DO 10	2123.98	41 408	1633	14	41 664	310	27	3094.17	**41 643**	**41 976**	18
DO 11	2157.58	43 297	1736	17	43 634	144	26	3130.44	**43 544**	**43 861**	15
DO 12	2221.96	46 794	1912	21	47 264	153	20	3195.25	**47 064**	**47 336**	16
DO 13	2256.73	49 221	2031	17	49 562	251	52	3237.65	**49 506**	**49 842**	19
DO 14	2345.39	54 164	2301	11				3311.09	**54 480**	**54 744**	13
DO 15.1	2355.17	54 940	2349	16				3322.24	**55 261**	**55 560**	11
DO 15.2	2366.15	55 737	2392	26				3329.72	**56 063**	**56 377**	14
DO 16.1	2398.71	57 988	2498	11				3350.44	**58 328**	**58 611**	9
DO 16.2	2402.25	58 210	2510	12	58 545	226	22	3352.59	**58 552**	**58 847**	14
DO 17.1	2414.82	59 018	2557	15	59 364	366	18	3360.02	**59 364**	**59 629**	17
DO 17.2	2420.35	59 386	2573	15	59 772	254	23	3363.42	**59 735**	**59 999**	25
DO 18	2465.84	64 049	2611	30				3388.73	**64 428**	**64 776**	15

CPD
10, 3537–3584, 2014

Table 2. Overview of CH_4 tiepoints for NH cooling events.

	NGRIP				WAIS-D			
	Depth (m)	Age (year bp)	Age uncert. (year)	Midpoint (year)	Depth (m)	Gas age (year bp)	Ice age (year bp)	Midpoint (year)
BA-YD	1524.20	12 775	136	81	2096.61	12 764	12 987	53
DO 3	1861.90	27 498	822	52	2747.24	27 516	27 905	41
DO 4	1882.60	28 548	887	17	2787.94	28 679	29 089	61
DO 5.1	1916.50	30 571	1010	70	2845.38	30 620	31 068	54
DO 5.2	1939.70	31 992	1108	13	2875.86	**32 169**	**32 580**	67
DO 6	1964.50	33 323	1192	37	2905.55	**33 508**	**33 891**	60
DO 7	1990.60	34 703	1286	13	2939.09	**34 897**	**35 289**	48
DO 8	2027.40	36 571	1401	21	2986.58	**36 776**	**37 163**	32
DO 9	2095.50	39 905	1572	42	3063.79	**40 131**	**40 482**	25
DO 10	2112.50	40 917	1621	44	3083.89	**41 150**	**41 504**	44
DO 11	2135.70	42 231	1685	27	3110.76	**42 472**	**42 816**	70
DO 12	2171.20	44 308	1783	41	3149.89	**44 562**	**44 899**	47
DO 13	2242.90	48 440	1996	27	3226.93	**48 720**	**49 060**	20
DO 14	2261.50	49 552	2052	20	3243.02	**49 839**	**50 172**	64
DO 15.1	2353.70	54 850	2339	18	3321.15	**55 171**	**55 465**	14
DO 15.2	2359.90	55 369	2370	55	3326.47	**55 693**	**55 981**	45
DO 16.1	2375.90	56 555	2435	49	3337.98	**56 886**	**57 219**	73
DO 16.2	2400.60	58 123	2508	15	3351.80	**58 464**	**58 756**	9
DO 17.1	2406.50	58 544	2530	35	3355.54	**58 888**	**59 154**	60
DO 17.2	2417.80	59 257	2570	18	3362.26	**59 605**	**59 865**	23
DO 18	2462.10	63 810	2611	14	3387.28	**64 187**	**64 551**	33

CPD
10, 3537–3584, 2014

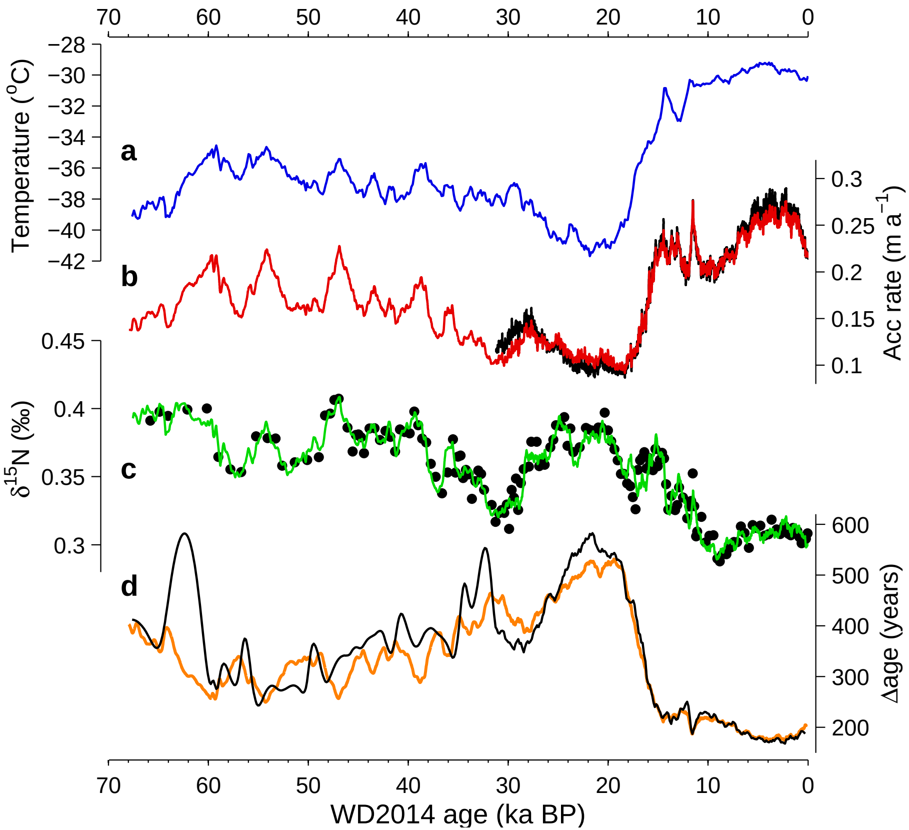

Figure 1. Modeling Δage for WAIS-Divide. **(a)** Past temperatures reconstructed from water δ^{18}O (100 year averages), calibrated to the borehole temperature profile. **(b)** Past accumulation rates as reconstructed by the firn densification inverse model (red), and from the annual layer count (black). **(c)** δ^{15}N data (black dots) with densification model output (green). **(d)** Δage calculated using the densification model (orange) and using the Parrenin Δdepth method (black) with constant 4 m thick convective zone and no correction for thermal δ^{15}N fractionation.

CPD
10, 3537–3584, 2014

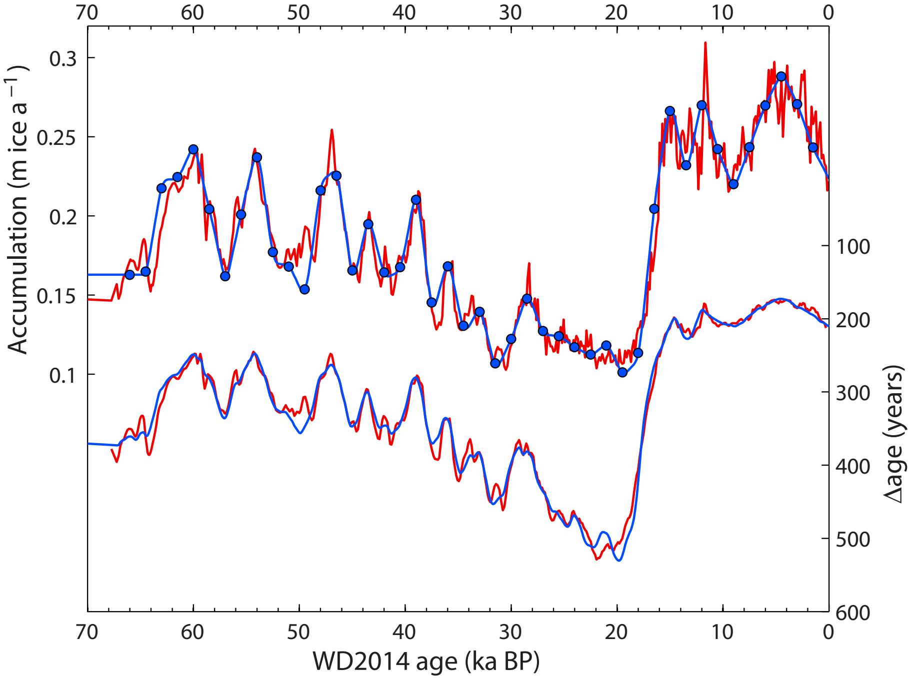

Figure 2. Reconstructing $A(t)$ and Δage from δ^{15}N: the choice of accumulation template. For the red curves we use the annual layer count $\lambda(z)$ as the basis for $A_{init}(t)$ during 0–31.2 ka BP, and δ^{18}O (i.e., the Clausius-Clapeyron scaling) as the basis for $A_{init}(t)$ during 34.2–68 ka. For the blue curves we use present day accumulation rates (A_{init} = 0.22 m a^{-1}) for the entire 0–68 ka interval. The function $\xi(t)$ is found as follows. We use control points at 1500 year intervals (blue dots); the algorithm has the freedom to change the value of $\xi(t)$ at each of these points. In between the control points $\xi(t)$ is found via linear interpolation.

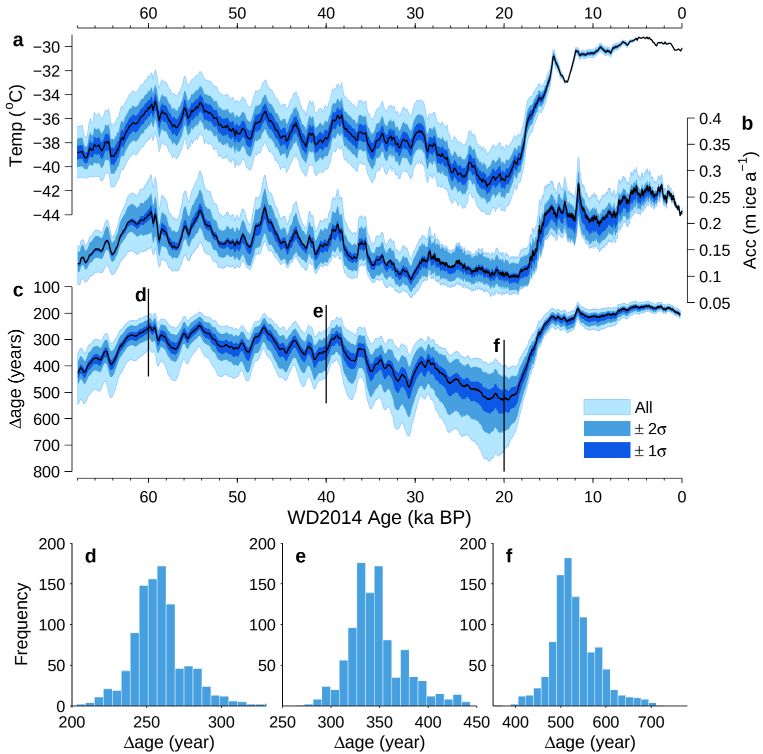

Figure 3. Δage sensitivity study. Shades of blue give the confidence intervals as marked; the dark curves represent the values used in the WD2014 chronology. **(a)** Temperature forcing of the densification model. **(b)** Reconstructed accumulation rates. **(c)** Reconstructed Δage. Histograms of Δage distribution are shown for **(d)** 60 ka BP, **(e)** 40 ka BP, and **(f)** 20 ka BP.

CPD
10, 3537–3584, 2014

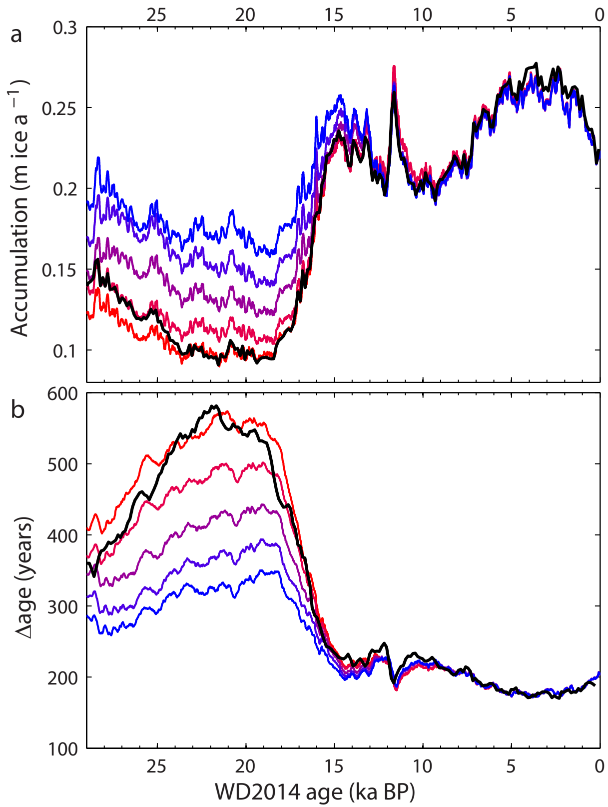

Figure 4. Impurity enhancement of densification rates at WAIS-D. Densification modeling results for **(a)** accumulation rates, and **(b)** Δage. We use Ca sensitivities $\beta = 0$ (red) through $\beta = 1 \times 10^{-2}$ (blue), in steps of 2.5×10^{-3} (shades of deep purple). Black curves give A and Δage from ice-flow modeling and $\lambda(z)$.

CPD
10, 3537–3584, 2014

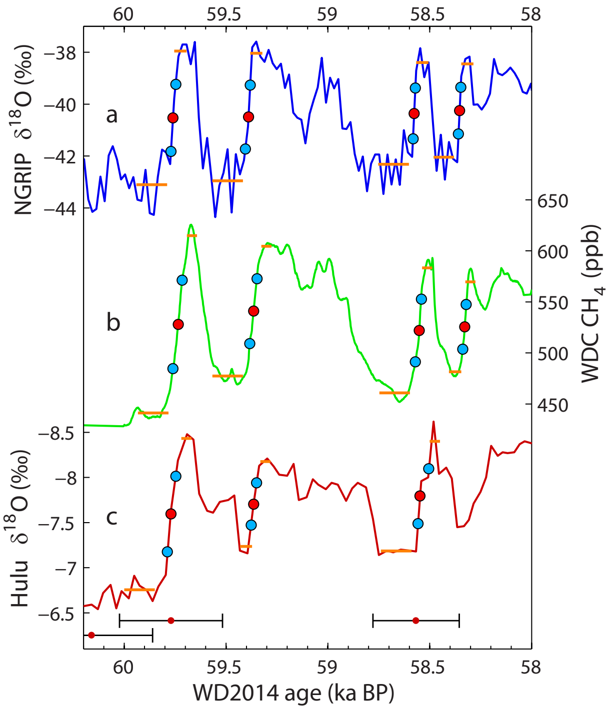

Figure 5. Determining the midpoint for the abrupt warming phases of DO 17 and DO 16 in **(a)** NGRIP $\delta^{18}O$ (on $1.0063 \times$ GICC05), **(b)** WAIS-D CH_4 (on WD2014) and **(c)** Hulu $\delta^{18}O$ with U/Th ages beneath the time series (red dots with error bars). Red dots give the midpoint (50 %) of the DO transition, the blue dots give the 25 % and 75 % marks in the DO transitions. The DO transition at 58.35 ka was not used in Hulu where it is much more gradual than in the other records (possibly because calcite sampling was not perfectly perpendicular to the stalagmite isochrones, or because growth rates were variable in between the U/Th ages).

CPD
10, 3537–3584, 2014

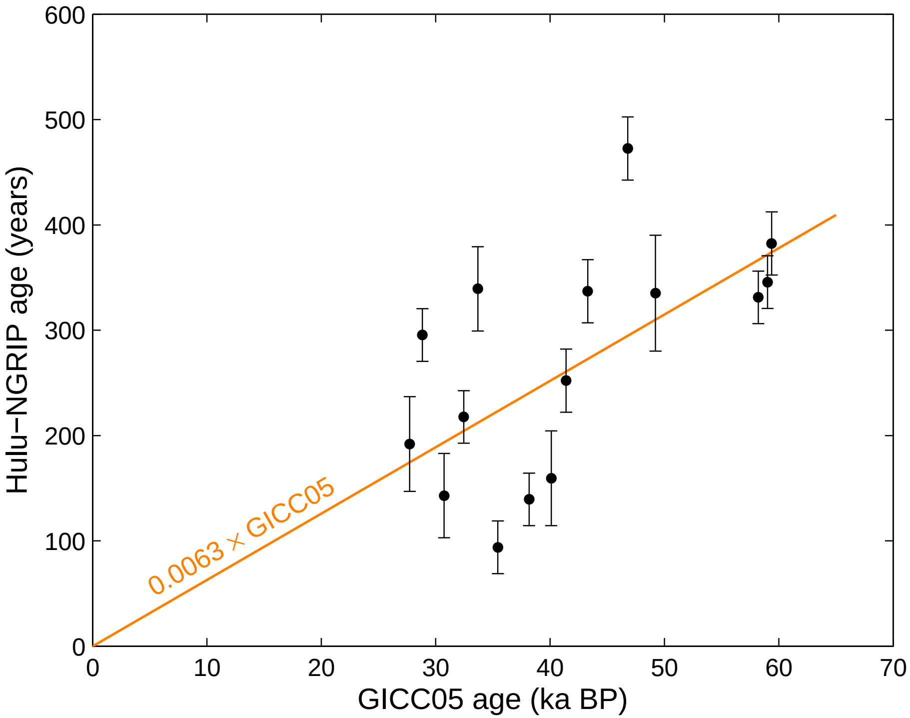

Figure 6. Hulu-NGRIP age offset at the midpoint of the DO $\delta^{18}O$ transitions. The error bars denote the root sum square of the midpoint determination uncertainty in NGRIP and Hulu $\delta^{18}O$ (Table 1). The GICC05 ages are placed on the BP 1950 scale, rather than the B2k scale (years prior to 2000 C.E.).

CPD
10, 3537–3584, 2014

The WAIS-Divide chronology – Part 2: Methane synchronization

C. Buizert et al.

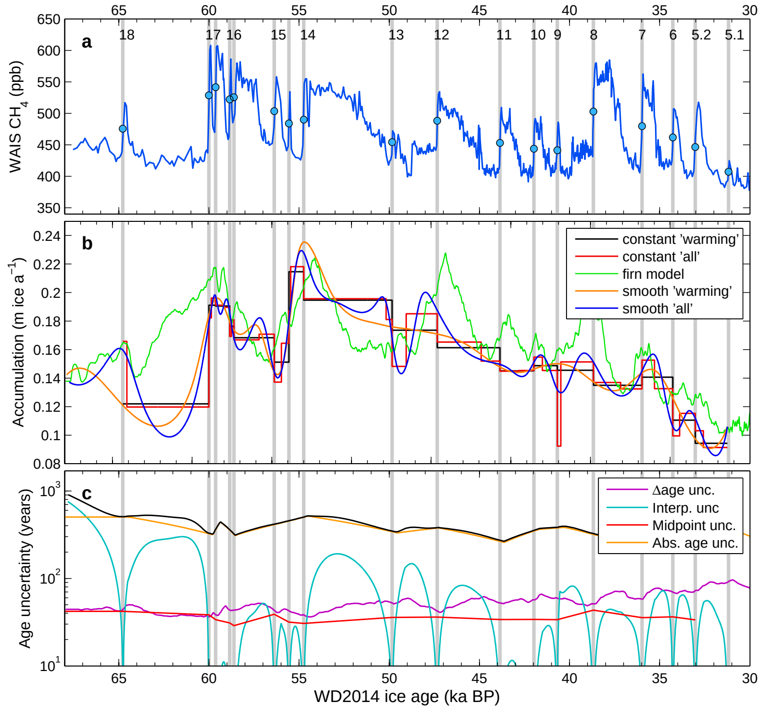

Figure 7. Interpolating between the CH_4 age constraints. **(a)** WAIS-D discrete CH_4 record with the abrupt stadial-interstadial transitions marked. DO numbering given at the top of the panel. **(b)** Different annual layer thickness scenarios, converted to an accumulation rate for comparison to the δ^{15}N-based firn model reconstructions. The age constraints used are either only the NH warming events ("warming"), or both the NH warming and cooling events ("all"). **(c)** Estimated 2σ uncertainties in the WD2014 chronology due to Δage, choice of interpolation scheme, midpoint detection, and the absolute age constraints used in the synchronization. Total ice age uncertainty is plotted in black.

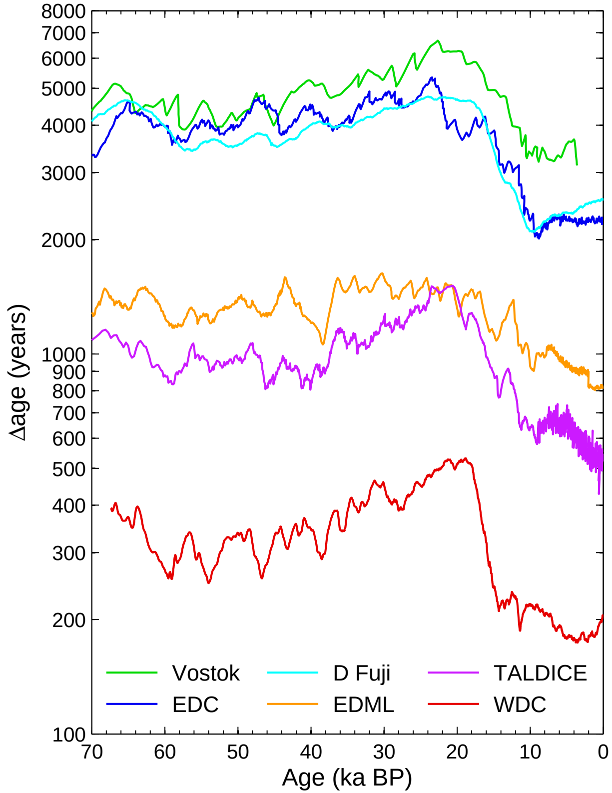

Figure 8. Comparison of Δage for different Antarctic cores, plotted on the gas-age scale. Dome Fuji Δage from Kawamura et al. (2007); WAIS-D from Sect. 3; all others from Bazin et al. (2013); Veres et al. (2013).

CPD
10, 3537–3584, 2014